JOURNAL OF MATERIALS SCIENCE 20 (1985) 2661–2686

Review
Microstructural aspects of superplasticity

B. P. KASHYAP, A. ARIELI, A. K. MUKHERJEE
Division of Materials Science and Engineering, Department of Mechanical Engineering, University of California, Davis, California 95616, USA

The microstructural aspects of the superplastic phenomenon are reviewed. The experimental results of a very large number of investigations are critically analysed in the context of: grain shape and size; grain growth; grain boundary sliding and migration, grain rotation and rearrangement; diffusion and dislocation activity. It is shown, that in spite of often conflicting evidence in the literature, a common pattern of microstructural behaviour emerges for all the materials and conditions investigated to date.

1. Introduction

There is now a fairly large number of metals and alloys that can deform extensively at elevated temperatures under small stresses without risk of premature rupture. These materials invariably have very fine grain sizes and the phenomenon is often referred to as micrograin superplasticity. Superplasticity has found application as a superior metal forming process in recent years. Therefore, currently both theoretical and experimental investigations emphasize precise structure-property correlations during superplastic deformation (SPD). The investigations on the microstructural aspect involve the role of: grain shape and size; grain growth; grain rotation and grain rearrangement; dislocation activity and the distinction between phase boundaries and grain boundaries in the SPD process.

Despite this progress and its impact on our knowledge of SPD, several microstructural issues remain unclarified. Significant among these issues are the role of grain growth specifically at low strain rates, the precise details of the process of accommodation at triple points due to grain boundary sliding (GBS) and migration, and the role played by dislocations in this deformation process in general and in the accommodation mechanism in particular.

Although some attempts [1–4] have been made to resolve these issues, no major breakthrough has been achieved in order to unravel the substructural details of the mechanism. There is still a lack of satisfactory correlation between microstructural and mechanical behaviour. This deficiency imposes a limitation in our ability to predict operative ranges in terms of stress–temperature–grain size–strain rate for the manifestation of SPD.

The present review integrates the available information on the microstructural aspects of the SPD, in search of some common pattern of microstructural behaviour in the reported results for all the materials and conditions investigated to date.

2. Initial microstructures

One of the prerequisites for micrograin superplasticity is a small (usually less than 10 μm) and equiaxed grain structure [1–4]. The initial microstructures in the as-worked (and short statically annealed) condition depend on alloy composition and thermo-mechanical treatment as described below.

2.1. Two-phase/multi-phase system

In two-phase or multi-phase alloy systems, the presence of a second phase increases the diffusion path needed for grain growth to occur. Therefore, small grains obtained by thermo-mechanical

0022–2461/85 $03.00 + .12

treatment in such alloys are relatively more stable. The grain size stability is enhanced by the increased difference between the diffusivity of the two phases and by the presence of more boundaries between dissimilar phases. The alloys containing a very large difference in the proportion of the two phases yield inhomogeneous microstructures and the recrystallization of as-worked structures can be obtained only after prolonged annealing.

2.2. Quasi-single phase

Several superplastic alloys have been developed recently on the principle that the presence of hard particles, e.g., intermetallic compounds or precipitates can pin the grain boundaries and thus inhibit the grain growth. However, such dispersion also influences the recrystallization behaviour during hot working or subsequent static annealing. Therefore unless the degree of working is adequate (above the required critical strain for recrystallization in the presence of impurities), the microstructures may not be fully equiaxed (in three mutually perpendicular directions).

2.3. Grain aspect ratio

In many cases the initial fine structures are not equiaxed [5–17]. Instead, the grains are elongated in one (linear orientation) or two (planar-linear orientation) directions as schematically shown in Fig. 1. Generally, the former results from extrusion or swaging while the latter results from rolling. Sometimes, agglomeration of small equiaxed grains of one phase in two-phase systems occurs along the working direction. Such microstructures are often referred to as banded structures. The characterization of elongated microstructures involves measurements in two or three mutually perpendicular directions [18, 19]. In superplastic literature the elongated grains were often characterized by the grain aspect ratio (GAR) of the longitudinal ($d_{\parallel}$) to transverse ($d_{\perp}$) dimensions of the grains. The dimensions $d_{\parallel}$ and $d_{\perp}$ are measured on metallographic sections taken parallel to the working direction. The value of GAR depends on alloy compositions and degree of working. Unfortunately, the degree of working is reported only in a few cases. For a 60/40 brass GAR was 1.5 [8], for an Al–Cu eutectic alloy about 1.8 [9] and about 4.67 for a Ti–6Al–4V alloy [10]. In a Pb–Sn eutectic alloy GAR values from 1 to 6 were reported depending on the thermo-mechanical treatment [17].

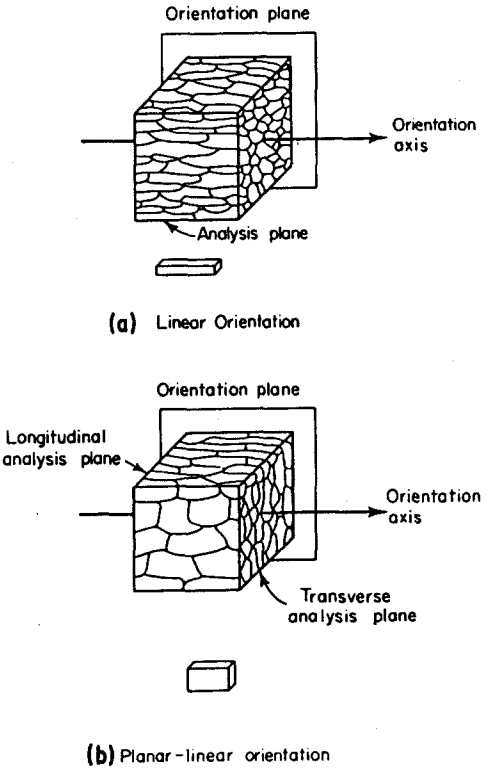

Figure 1 Schematic microstructures obtained typically after working (a) linear orientation, and (b) planar-linear orientation [18].

3. Microstructural instability

The concept that the initial microstructures remain unaltered during SPD is no longer valid. The instability may be broadly divided into: (a) change of as-worked (also short statically annealed) unstable microstructures and (b) changes associated with micro-mechanisms of deformation. The former type of change will be described in this section while the latter will be described in Section 4. Superplastic deformation causes the evolution of elongated grains towards equiaxed grains, grain growth and redistribution of the phases.

3.1. Evolution towards equiaxed grains

The presence of elongated grains results in initially higher values of the flow stresses [8, 12, 14, 17] and lower values of the strain rate sensitivity coefficient, m [12, 15]. The elongated structure gradually evolves toward an equiaxed structure during the early part of the deformation, stabilizing at GAR $\simeq$ 1.2 [8–10]. The strain at which a stable, equiaxed structure is achieved depends on the alloy system, initial GAR, test temperature

TABLE I Strains where an equiaxed structure is achieved for various superplastic alloys

Alloy	Engineering strain (%)	Reference
Al–Cu–Zr	~ 50	[20]
60/40 Brass	< 30	[8]
Cu–P	< 30	[13]
Cu–Zn–Fe	< 40	[14]
IN-744	< 80	[15]
Al–Cu eutectic	~ 15	[21]
Pb–Sn eutectic	~ 5	[22]
Ti–6Al–4V	0*	[10]

*Static annealing at the test temperature.

and strain rate. The values for such strain level experimentally observed in different alloys are listed in Table I. Also, it might be suggested that the strain values, beyond which the equiaxed structure is achieved, will vary for the same alloy with different thermo-mechanical histories.

The decrease in GAR results in strain softening. Both lower [21] and higher [22] m-values than those obtained during steady-state deformation are reported in the literature for the initial stages of the deformation. However, usually no attempt was made in the original investigations to correlate them with the concomitant microstructural changes.

Watts *et al.* [20] investigated structural changes in a pre-aged Al–Cu–Zr alloy following SPD. After 10% strain, the subgrain size in the originally polygonized regions increases by an order of magnitude to ~ 3 μm. After 50% strain a uniform equiaxed grain structure is attained and the size of the subgrains equals the grain size.

Usually, once an equiaxed grain structure is achieved it remains so even after hundreds or thousands % of strain [17, 20, 23–30] in the superplastic regime. However, in some investigations, slight grain elongation in region II are reported [31–33] in the initially equiaxed microstructures. Valiev and Kaibyshev [31], working with two alloy systems, Zn–1% Al and Mg–1.5% Mn–0.3% C [32], found that the grain elongation increases as the strain rate decreases. Lee and Niessen [34], in their investigation of the Zn–0.1% Ni–0.04% Mg alloy, found that the grain elongation in region II was about 17.5% of the total elongation of the specimen. It is worth noting that all the investigations showing grain elongation during superplastic flow were carried out with single phase alloys except that investigated by Ghosh and Hamilton [35] where the alloy was a duplex phase, $\alpha + \beta$ titanium alloy (Ti–6Al–4V). In region III, where dislocation creep is believed to be the rate-controlling mechanism, grain elongation is expected to occur and indeed is observed [17, 24, 36, 37].

3.2. Grain growth

Another important microstructural feature now firmly established, is that grain growth takes place concurrently during SPD [5–7, 9–12, 17, 20, 21, 23, 29, 30, 32, 35, 38–72]. This is illustrated in Fig. 2 where the grain growth as a function of strain is depicted for both α and β phases in a Ti–6Al–4V alloy [72].

The grain growth during SPD results from: (a) static annealing at the elevated temperature environment for the duration of the deformation, and (b) strain enhanced growth due to deformation *per se*. In Fe–25.7Cr–6.6Ni at 1000° C, the grain size obeys the grain growth kinetic of the form [70]

$$d \propto t^{0.49} \simeq t_s^{0.19}\dot{\epsilon}^{0.29} = t_s^{0.19}\dot{\epsilon}^{0.29}t_\epsilon^{0.29} \cong \dot{\epsilon}^{0.29}t^{0.48} \quad (1)$$

when deformed at a strain rate of 1×10^{-4} sec^{-1}. Here d is the grain size. t, t_s and t_ϵ are time in minutes corresponding to combined, static and dynamic annealing respectively and $\dot{\epsilon}$ is the strain rate. Several workers concluded that the factor governing the post-deformation grain size is the time at the test temperature and not the strain [9, 10, 66, 73]. In these investigations, the effect of deformation was to enhance the grain growth process by the same factor regardless of the exact values for strain and strain rate.

In an effort to isolate the effect of the strain rate on the grain growth rate, Clark and Alden [52] used the "growth enhancement parameter = $\Delta d/d_a$", where Δd is the difference between the grain size after deformation, d, and the grain size of a specimen statically annealed at the deformation temperature for an equal time, d_a. Their results show that $\Delta d/d_a$ increases with strain, the rate of grain growth reaching a maximum at intermediate strain rates, Fig. 3a. Kaibyshev *et al.* [61] investigated grain growth in Zn–0.4% Al over three orders of strain rates. The rate of grain growth due to deformation increased with increasing strain rate as shown in Fig. 3b. Wilkinson and Caceres [74] analysed the data on several superplastic materials as shown in Fig. 3c. At intermediate strain rate, the rate of grain growth

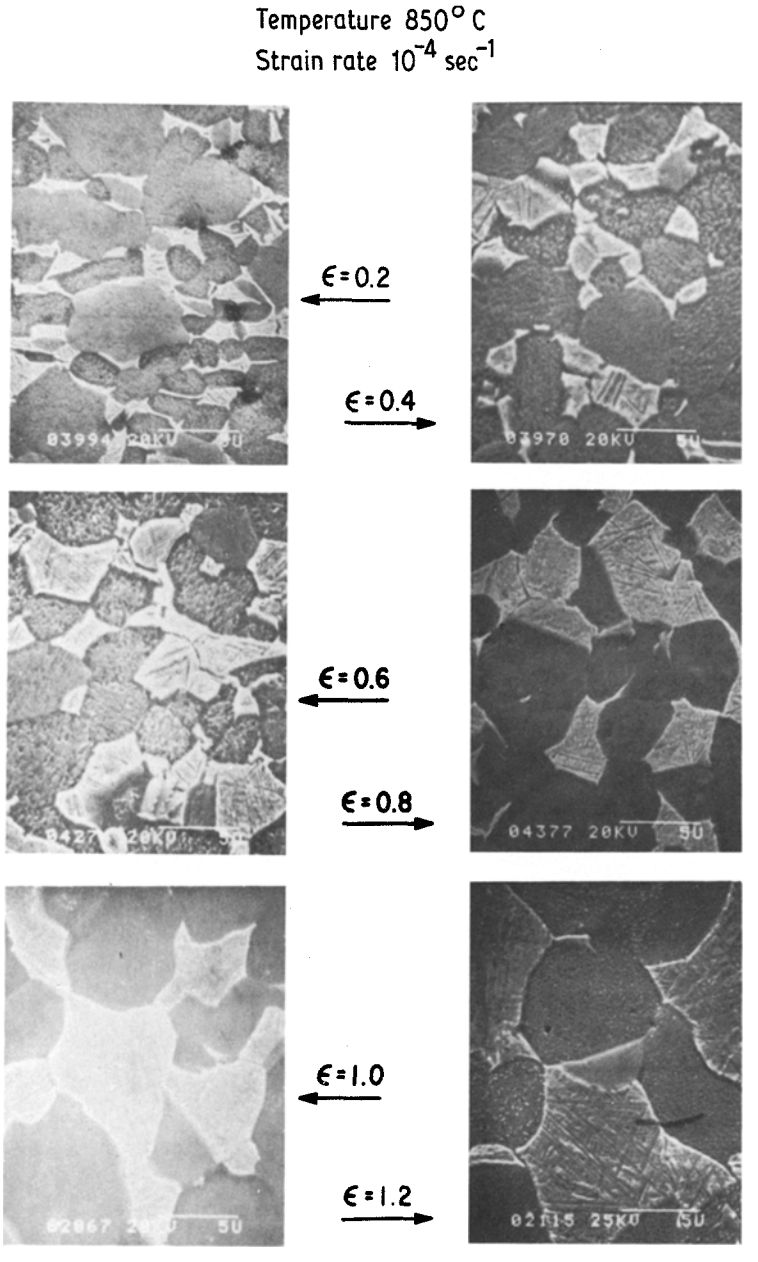

Figure 2 Microstructures exhibiting grain growth in α/β microduplex Ti–6Al–4V alloy after ‹astic deformation to ıt levels of strain [72].

seemed to be linearly dependent on strain rate. At lower and higher strain rates the rate of grain growth appears to be relatively insensitive to strain rate (often reaching a plateau). It has been suggested that grain growth during SPD is associated with increasing grain boundary mobility as a consequence of increasing vacancy concentration. This suggestion finds support in the experimentally measured [75] dependence of the vacancy concentration on strain-rate as shown in Fig. 3d.

Another factor which must be considered in discussing the grain growth is the rate of growth of the different phases present in the duplex superplastic alloys. The data presented by Samuelsson *et al.* [60] on the grain growth of both α (Al-rich) and β (Zn-rich) phases in a Zn–40% Al alloy were analysed. The ratios of final grain sizes to initial grain sizes increase with decreasing strain rate as shown in Fig. 4. This is due to the dominant effect of static annealing at lower strain rates.

3.3. Phase redistribution and change in the phase proportion

Evolution of elongated microstructures towards

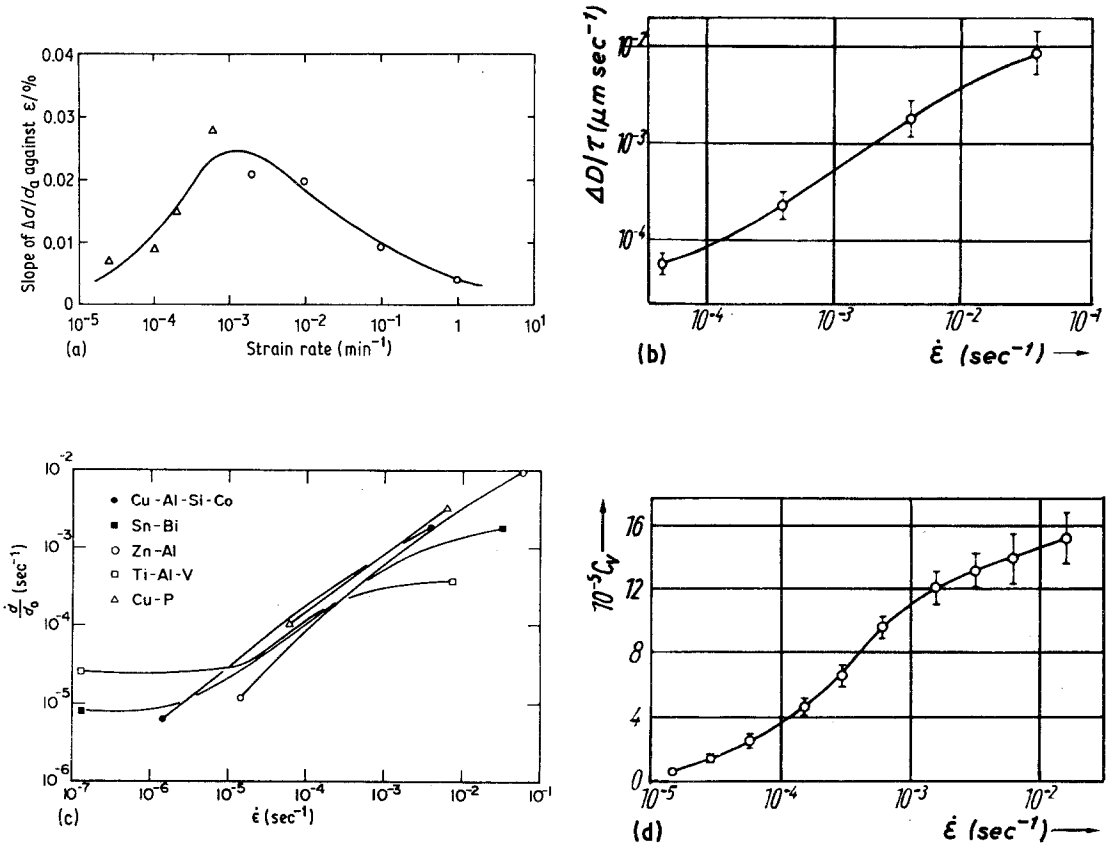

Figure 3 (a) The variation of the "growth enhancement parameter" with strain rate [52]. (b) The strain rate dependence of the rate of grain growth $\Delta D/\tau$ [61], where ΔD is the change in grain diameter (μm) during the time interval (seconds). (c) The strain rate dependence of the rate of grain growth normalized by the initial grain size d_0 for various materials [73]. (d) The strain rate dependence of the excess vacancies Δc_v in the Zn–0.4% Al alloy [74].

equiaxed microstructures in a two phase alloy system results in producing more neighbours which are of opposite phase-types. The redistribution and transformation to equiaxed shape in a Pb–Sn eutectic alloy [76] after SPD is shown in Fig. 5. In several investigations of different alloys the occurrence of concurrent grain growth is also noticed [19]. The initially banded microstructures tend to attain a more uniform configuration among the grains of different phases along with concurrent grain growth as illustrated for Cu–5P alloy [11] in Fig. 6. Dunlop and Taplin [49] investigated microstructural aspects of deformation over a range of strain rates encompassing the three regions of superplastic deformation in an aluminum bronze. In the lower strain rate range, below that for high values of m, clumps of grains slide together as units. With increasing strain rate, through and beyond the strain rate range where peak values of m are recorded, the tendency for the clumps of grains to slide together decreases. In a banded structure, therefore, the uniform redistribution among grains of different phases may occur faster at the higher strain rates than that at the lower strain rates. At lower strain rates, for the same strain level, more grain growth (combined static and dynamic type) occurs and the extent of phase redistribution is less.

Some alloys become difficult candidates for investigating superplastic behaviour due to changes in the phase proportions. The phase proportions vary primarily due to the difference in test temperatures as reported in α/β brass [51], Ti–6Al–2Sn–4Zr–2Mo–0.1Si [77] and Ti–6Al–4V alloys [78]. For example in Ti–6Al–2Sn–4Zr–2Mo–0.1Si, as compared with the as-received material the approximate vol% of primary α increased [79] from 50 initially to 55 and then to 70% as a result of deformation at 927 and 899°C respectively, Fig. 7. This change is insensitive to strain rate.

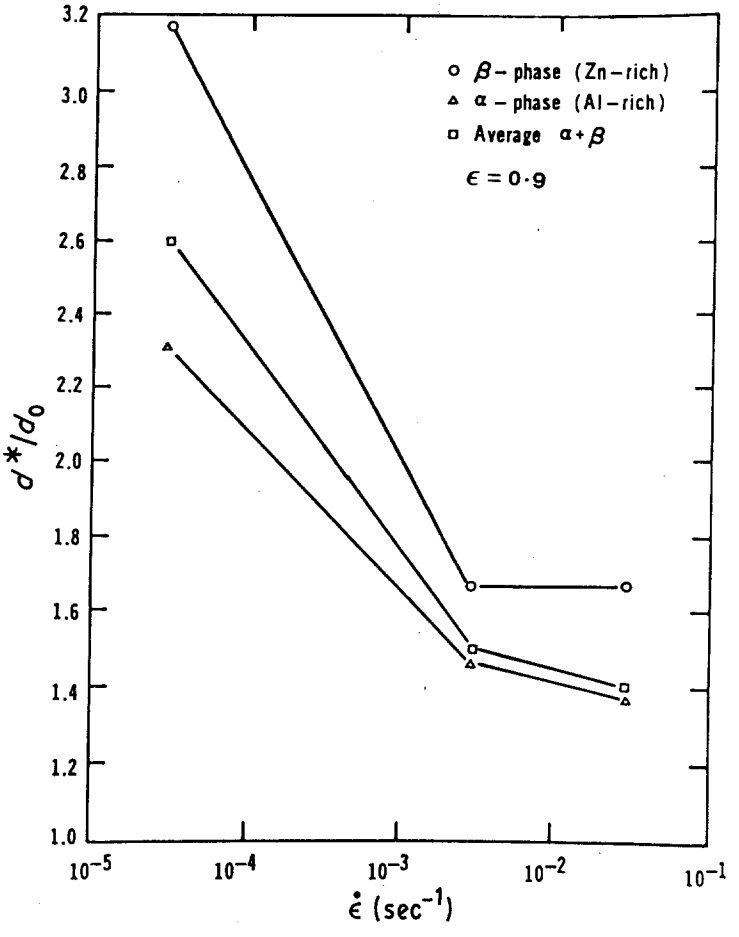

Figure 4 The strain rate dependence of the growth of constituent α and β phases in Zn–40% Al alloy [60].

4. Microstructural changes associated with deformation mechanisms

The studies of high temperature deformation of superplastic materials over the three regimes show that GBS, diffusion and dislocation activity operate up to different extents. Fig. 8 illustrates the proportions of these mechanisms in the different regimes for two alloys [80]. The contributions of the operative mechanisms are shown in Fig. 9 as a function of strain rate at different temperatures in a Zn–Cu–Mn alloy [81]. These mechanisms along with other associated phenomena will be described below.

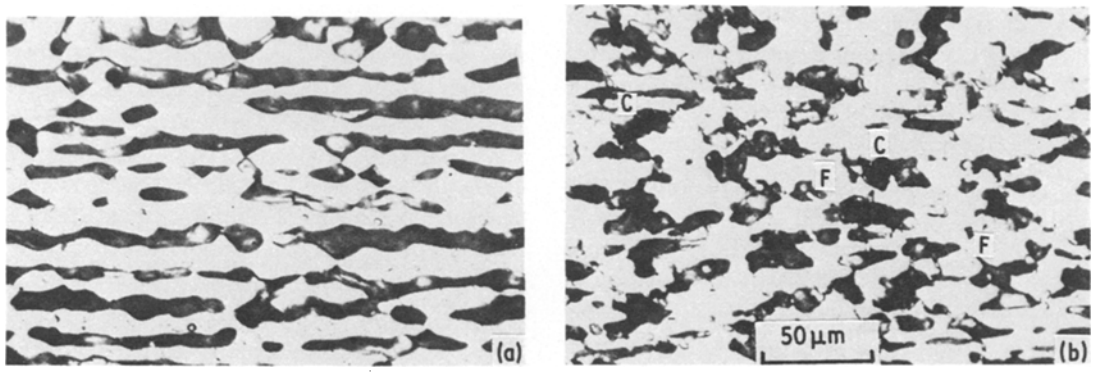

Figure 5 Evolution of equiaxed microstructures in the Pb–Sn eutectic from initially elongated microstructures [75]; (a) undeformed, (b) strained 175% in tension parallel to the stringers in (a). Note: c, curved interphase boundaries with cusps; F, finger-like protuberances.

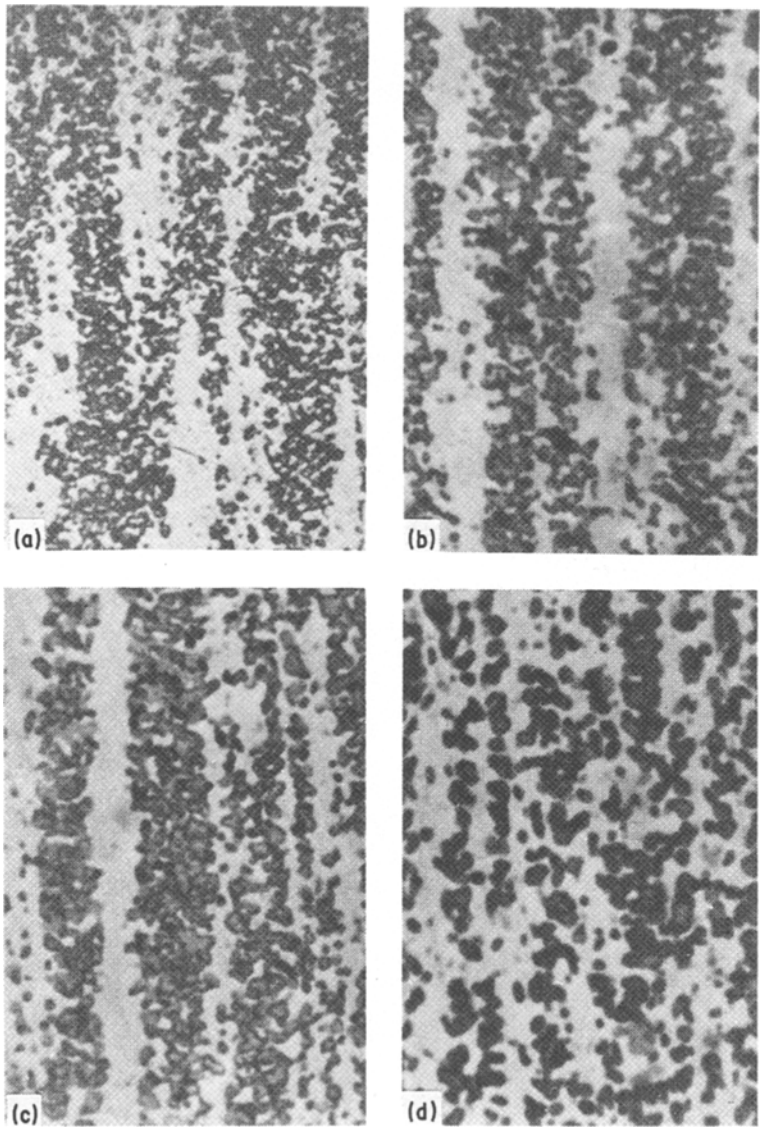

Figure 6 Cluster break-up and coarsening of the β-phase (dark) observed on longitudinal sections of the Cu–5P alloy deformed at a constant strain rate of 1.28×10^{-4} sec^{-1} at 550° C after true strains [11]: (a) 0%; (b) 18%; (c) 47%; and (d) 70%.

4.1. Grain boundary sliding

Extensive interface (either grain or phase-boundary) sliding is commonly observed during superplastic flow. Even in investigations where diffusional creep was found to be the dominant mechanism, GBS is expected to accompany the diffusional creep [82–85]. The contribution of GBS to total elongation are summarized in Table II for different materials. The results shown in Table II are based on different techniques for measuring GBS [93]. This makes direct comparison difficult. However, the general trend is the same in every investigation: the contribution of GBS is a maximum in region II and decreases at higher (region III) and lower (region I) strain rates.

Only very limited works were performed to distinguish the sliding boundaries (α–α, β–β, α–β, etc) [89, 92, 94] or to investigate the effect of the orientation of the sliding boundary relative to the applied stress [32].

Chandra *et al.* [94] measured grain and phase boundary sliding at various interfaces in an α/β

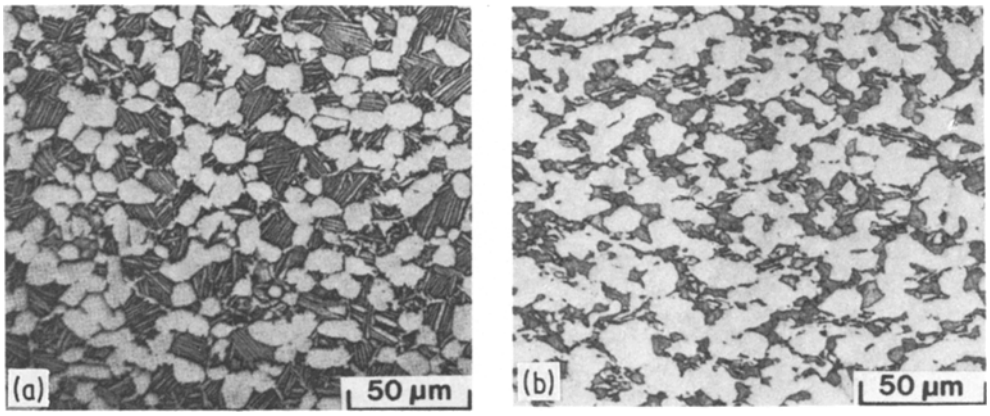

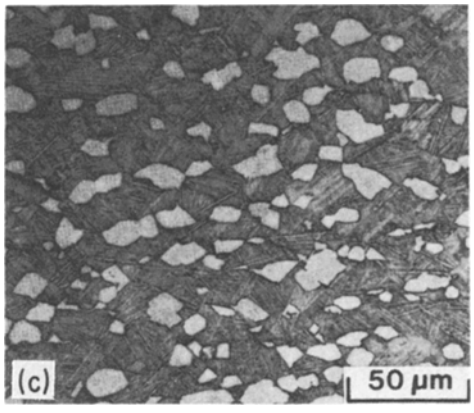

Figure 7 Microstructures of the $(\alpha + \beta)$ Ti–6Al–2Sn–4Zr–2Mo–0.1Si alloy; as-received; (b) deformed ($\epsilon \simeq 0.7$) at 899° C; and (c) deformed ($\epsilon \simeq 0.7$) at 982° C, $\dot{\epsilon} = 10^{-3}$ sec^{-1} [79].

brass, and found that sliding occurred on α–β boundaries more readily than on α–α and β–β interfaces. Their results are shown in Table III.

Vastava and Langdon [89] measured the contribution of the individual boundaries in a Pb–Sn eutectic alloy at strain rates of 3.33×10^{-6} sec^{-1} (region I), 1.33×10^{-3} sec^{-1} (region II), and 1.33×10^{-1} sec^{-1} (region III). For all three regions they found that sliding took place predominantly at the Sn–Sn boundaries and absolutely no sliding occurred at the Pb–Pb boundaries. The extent of sliding at the Pb–Sn interphase boundaries was intermediate between those in Sn–Sn and Pb–Pb grain boundaries. Their results are summarized in Table IV. Shariat *et al.* [92] further evaluated the roles of grain and interphase boundary sliding in two-phase superplastic alloys. In Zn–22% Al, maximum sliding tends to occur at the Zn–Zn intercrystalline boundaries, there is slightly less sliding at the Zn–Al interphase boundaries, and sliding is minimal at the Al–Al intercrystalline boundaries. The GBS data on the Pb–Sn eutectic

TABLE II Contribution of grain boundary sliding to the total axial strain (ϵ_{gb}/ϵ_t) in regions I, II and III

Material	ϵ_{gb}/ϵ_t (%)			Reference
	Region I	Region II	Region III	
AMg6 Alloy	~ 50	~ 70	~ 40	[80]
Al–33% Cu eutectic	–	~ 70	–	[86]
Al–9% Zn–1% Mg	42	63	26	[63]
Al–11% Zn–1% Mg	~ 60	~ 80	~ 50	[37]
MA8	~ 50	~ 75	~ 50	[30]
Mg–33%Al eutectic	12	64	29	[46]
Mg–1.5% Mn–0.3%C	33	41–49	30	[32]
Pb–Tl	–	50	33	[25]
Pb–Sn eutectic	–	~ 70	–	[88]
Pb–Sn eutectic	21	56	20	[89]
Pb–Sn eutectic	–	50	–	[90]
Zn–0.4% Al	42	48	28	[61]
Zn–Al eutectoid	~ 30	~ 60	~ 30	[37]
Zn–Al eutectoid	< 30	~ 60	< 20	[91]
Zn–Al eutectoid	10	11	6	[92]

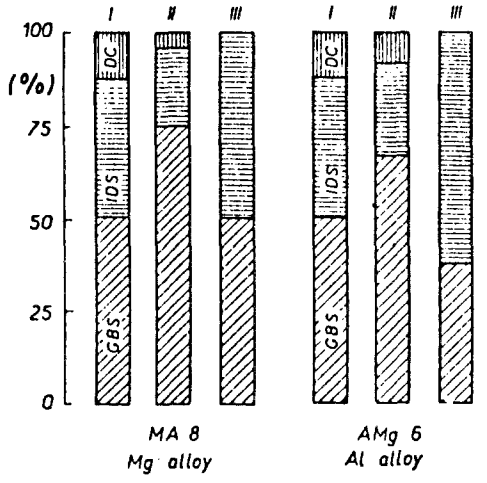

Figure 8 Contribution of grain-boundary sliding (GBS), intragranular dislocation slip (IDS) and of diffusion creep (DC) to the total deformation of the MA8 and AMg6 alloys in different regions of the superplastic curve [80].

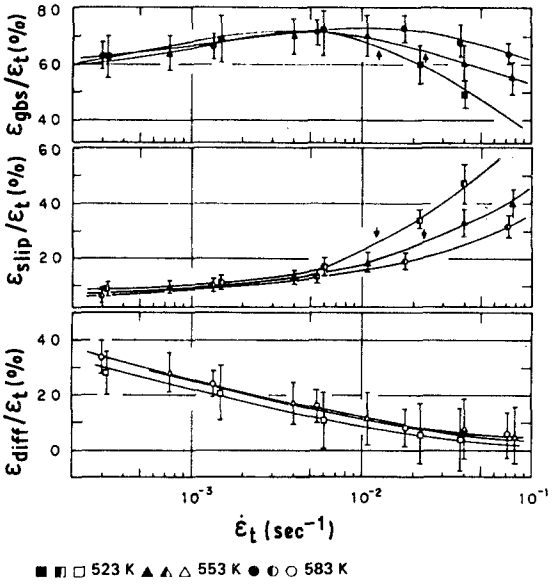

Figure 9 Contribution of grain boundary sliding, slip, and diffusional flow to total specimen elongation at different strain rates and temperatures in a Zn–Cu–Mn alloy [18]. Arrows indicate maximum strain rates for superplasticity.

and Zn–Al eutectoid alloys led to the suggestion [92] that the maximum sliding occurs on the interfaces which have the highest values of δD_{gb}. Here δ is the width of the boundary and D_{gb} is the grain boundary diffusion coefficient.

Valiev and Kaybyshev [32] found a strong dependence of the amount of GBS on the angle between the axis of the specimen and the sliding boundary trace on the surface.

In region I sliding occurred mainly at the transverse boundaries, whereas in regions II and III the largest amount of sliding was measured at boundaries lying at 45° to the specimen's axis. Also in regions II and III the sliding anisotropy was less marked than that in region I. In all the three regions the boundaries which exhibited the largest amount of sliding also showed the most active boundary migration. Fig. 10 summarizes these results.

4.2. Grain boundary migration

Grain boundary migration is important from both the diffusion and GBS point of view. As Ashby [95] pointed out, "sliding without change of boundary structure is possible only if the boundary also migrates." The GBM usually accompanies the superplastic flow. Fig. 11 illustrates the occurrence of GBM in sliding Sn–Sn boundaries in a Pb–Sn eutectic alloy [89]. Although the assumption that GBM accommodates GBS at triple points [24, 46] is open to debate, the occurrence of GBM during superplastic flow is well documented in several works [24, 32, 37, 46, 76, 96, 97]. Nicholson [96] reported precipitate free zones (PFZ's, also called denuded zones) near both grain (α–α) and interphase (α–β) boundaries in a Zn–Al eutectoid alloy.

Similar PFZs were observed in Mg–alloys by Karim *et al.* [98] and Lee [24] who interpreted them in terms of diffusional creep and GBM, respectively. An example of PFZs is shown in Fig.

TABLE III Grain and phase boundary sliding at various interfaces in α–β brass (average grain size = 32 μm) strained at 600° C and $\dot{\varepsilon} = 7.7 \times 10^{-5}$ sec^{-1} [94]

Type of boundary	Sliding rate (cm sec^{-1})	Corresponding strain rate (sec^{-1})
α–α	8.6×10^{-8}	2.69×10^{-5}
α–β	1.5×10^{-7}	4.69×10^{-5}
β–β	6.8×10^{-8}	2.13×10^{-5}

TABLE IV Results obtained from sliding measurements [89] on Pb–Sn eutectic over the three regions of the superplastic curve

	Extent of sliding (μm)			
	Boundary type			Average for all boundaries
Region	Sn–Sn	Pb–Sn	Pb–Pb	
I	0.33	0.27	0	0.30
II	0.87	0.43	0	0.79
III	0.34	0.22	0	0.28

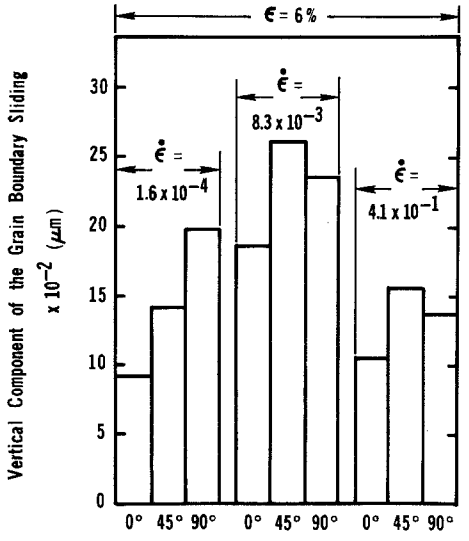

Figure 10 The value of the vertical component of the grain boundary sliding, h, versus boundary angle with the tensile axis [32]; (a) $\dot{e} = 1.6 \times 10^{-4}\,\text{sec}^{-1}$ (region I); (b) $\dot{e} = 8.3 \times 10^{-3}\,\text{sec}^{-1}$ (region II); (c) $\dot{e} = 4.1 \times 10^{-1}\,\text{sec}^{-1}$ (region III).

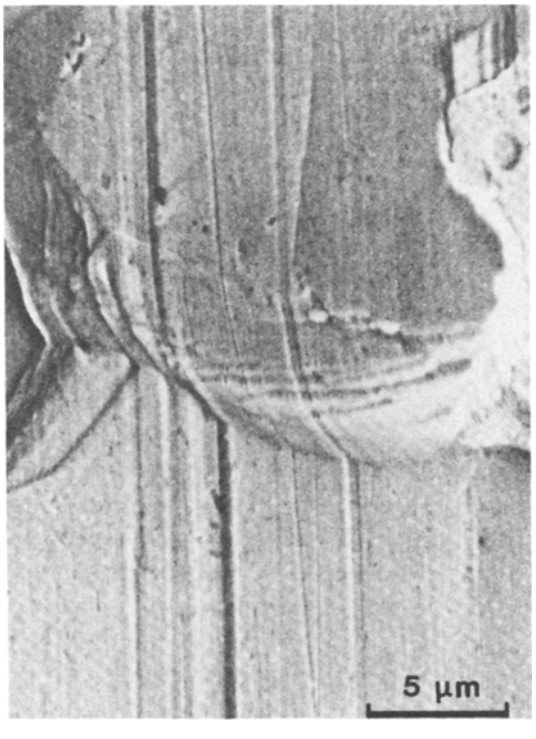

Figure 11 Grain Boundary sliding accompanied by grain boundary migration at Sn–Sn boundaries in a Pb–Sn eutectic alloy [89].

Figure 12 Precipitate free zones (PFZs) observed near grain boundaries in a Mg alloy [98].

12. Lee [46] put forward an explanation where GBS is followed by GBM at triple points to minimize boundary energy, Fig. 13. As a result, two adjacent grain boundaries will have opposite curvatures, Fig. 13, and this will explain the curved boundaries usually observed after SPD as illustrated in Fig. 14. The initially straight boundaries (Fig. 14a) take a curved shape [56] (Fig. 14b) or the grains appear bulbous [99] (Fig. 14c) after SPD. Such opposite curvatures were also observed in a Zn–22% Al alloy, where the α-phase has convex sides and the β-phase has concave sides, and in an Al–Cu eutectic, where Al_2Cu has convex sides whereas Al grains have concave sides [96].

Lee's model, however, cannot account for the bulbous aspect of the previously straight boundaries (Fig. 14c). A possible explanation then might be that additional components of GBM are activated due to [100, 101] dislocation activity in the mantle. In contrast to surface energy-induced boundary migration, the strain-induced boundary migration takes place in such a way that the boundary moves away from its centre of curvature [100] and usually has an irregular curved shape [100, 101] Fig. 15. The moving boundary leaves behind a region which is cleaner, as the migrating boundary usually drags away impurity atoms [102]. A migrating boundary

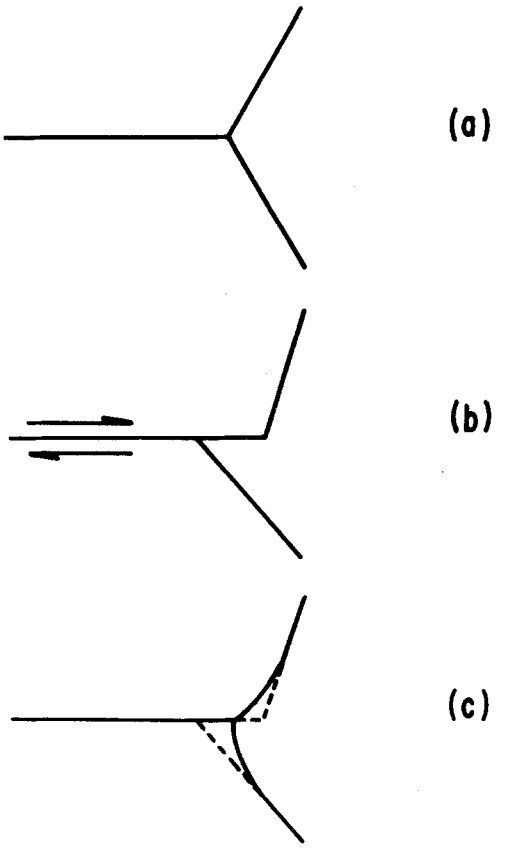

Figure 13 Schematic diagram showing the mechanism by which the boundaries become curved. (a) Initial state, (b) after sliding, (c) after separation at triple points [46].

affects the superplastic flow because its diffusivity will differ from the diffusivity of a stationary boundary [103, 104].

4.3. Grain rotation and grain rearrangement

4.3.1. Grain rotation

Appreciable grain rotations have been observed during superplastic flow. Experiments showing evidence of grain rotations consisted of: (a) deformation of prepolished and etched specimens with marker lines inscribed on the surface [20, 37, 39, 88] or (b) *in situ* deformation [105–107]. The main characteristics of grain rotation seems to be that they never rotate more than 45°. The rotations often change sign during the deformation [105, 106] (Fig. 16) indicating that the sense of rotation for any one grain depends on its instantaneous surroundings.

TABLE VI Relative frequency of grain rotation as a function of strain at $\dot{\epsilon} = 1.12 \times 10^{-4}$ sec^{-1} [63]

	Relative frequency (%)				
	Rotation angle (degrees)				
ϵ (%)	0–5	5–15	15–25	25–35	35–45
30	53	34	10	3	0
60	50	40	8	2	0
100	44	37	14	3	2
200	42	34	14	6	4

Beere [108] assumed that grain rotation arises from different sliding rates at different types of boundaries. By further analysing the data on grain rotations measured by Geckinli and Barrett [105], Beere concluded that in order to account for the maximum rate of rotation observed experimentally, the sliding rate must vary by a factor of 10. In view of the measured sliding rates at various types of boundaries by Chandra *et al.* [94], this value appears to be reasonable.

Matsuki *et al.* [63] measured the amount of grain rotation during SPD as a function of strain rate and strain. Their results are summarized in Tables V and VI.

It is interesting to note that rotations higher than 35° were observed only at the lowest strain rate. As the strain rate was increased, but still in region II, the relative frequency of the intermediate degrees of rotation (5–25°) increased to 48% compared to only 30% at lower strain-rate. In region III, the relative frequency for rotation through intermediate degrees (5–25°) dropped to 23%, whereas most of the rotation was limited to less than 5° (75%).

As the strain increases from 30 to 200% more grains rotate to larger degrees. This is also shown in Fig. 17. The grain rotation will not contribute to the total strain, but might provide an additional

TABLE V Relative frequency of grain rotation as a function of strain rate at $\epsilon = 60\%$ [63]

Region	$\dot{\epsilon}$ (sec^{-1})	Relative frequency (%)				
		Rotation angle (degrees)				
		0–5	5–15	15–25	25–35	35–40
II	3.33×10^{-5}	65	25	5	3	2
II	1.12×10^{-4}	50	40	8	2	0
III	1.83×10^{-3}	75	20	3	2	0

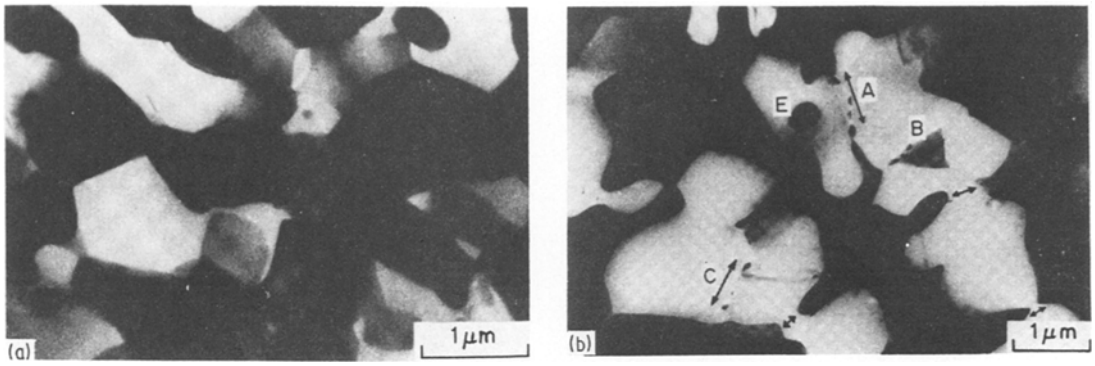

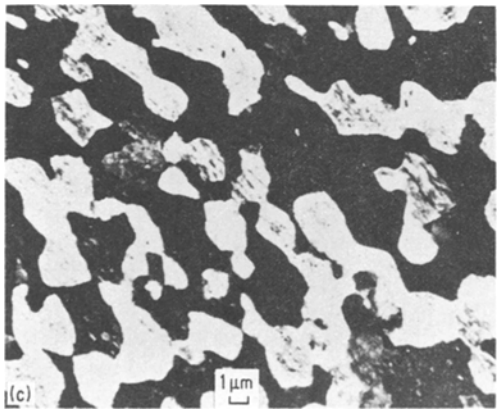

Figure 14 (a) 100 kV TEM micrograph showing straight grain and phase boundaries in the specimen's grip (undeformed) region [56]. (b) Curved interface boundaries after 30% superplastic flow [56]. (c) TEM micrograph showing the "bulbous" aspect of the interphase boundaries after 1280% superplastic flow [99].

degree-of-freedom during SPD. During deformation, the grain rotation together with GBS will lead to an overall reduction in texture [1].

4.3.2. Grain rearrangement

Grain rearrangement takes place to a large extent during SPD and two grains which are initially neighbours may end up being many grain diameters apart after SPD. Grain rearrangement is facilitated by grain rotation [108]. The micrographs in Fig. 18 illustrate sequence of grain rearrangement during SPD of Pb–Sn eutectic at 25° C [109]. The formation of transitory surface voids and their elimination by the grain emergence can be noticed by comparing the microstructures at increasing level of strain. The microcreep curves between randomly selected grains were estimated from a series of micrographs (as in Fig. 18) by Rai and Grant [109] and the results are shown in Fig. 19.

The relative motion of the adjacent grains seems to depend on the orientation of their common boundary [105]. Grains with their boundaries making angles of 0° or 90° with the tensile axis, move less rapidly than other grain orientations. In view of the sliding anisotropy observed in superplastic flow [32, 61], the grain rearrangements

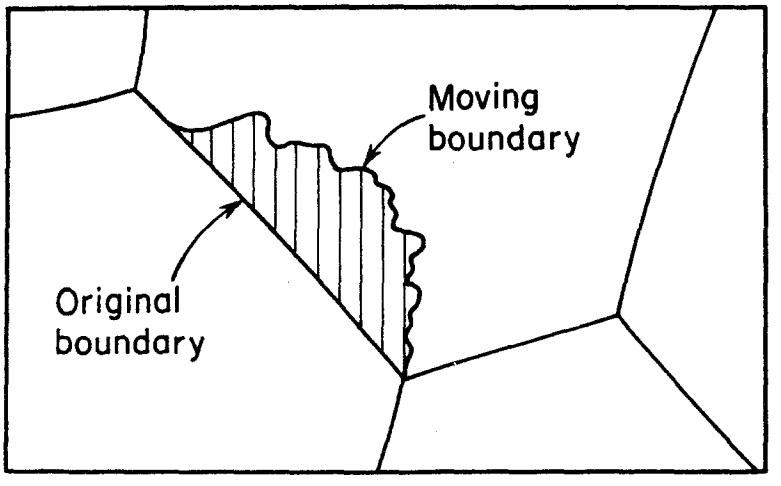

Figure 15 Schematic representation of strain induced boundary migration [100].

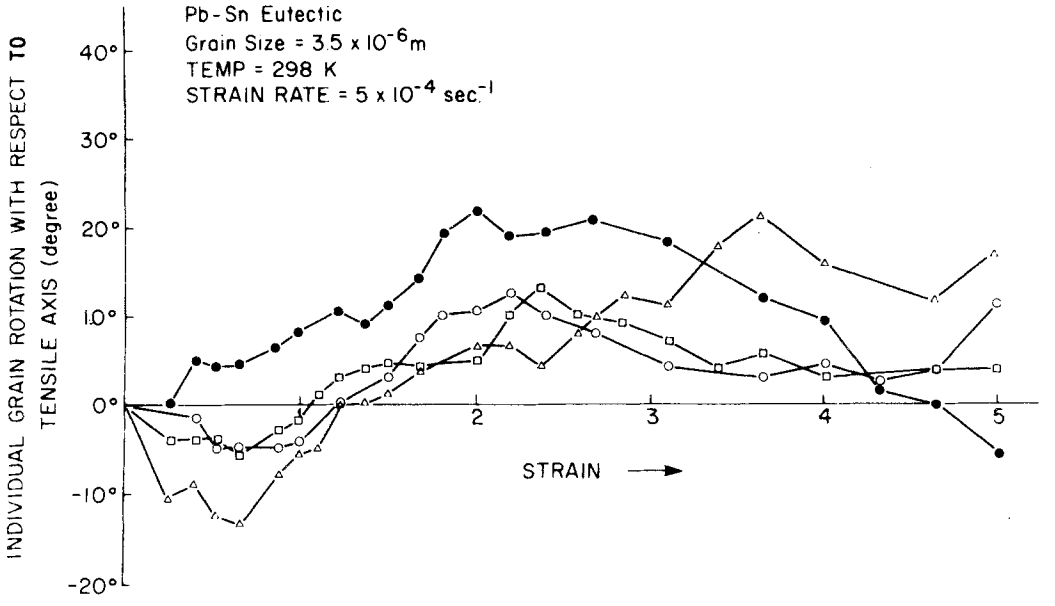

Figure 16 Direction and extent of grain rotation against strain [105].

seem to be governed by GBS. Naziri *et al.* [56, 110] carried out *in situ* tensile straining, in a 1 mV electron microscope, of thin foils of an Zn–Al eutectoid alloy. Their observations clearly demonstrate that extensive grain rearrangement takes place during straining (Fig. 20), thereby verifying a model for "grain-neighbour switch" as put forward by Ashby and Verrall [111]. This type of grain rearrangement was subsequently observed in another *in situ* TEM investigation by Kobayashi *et al.* [112] on an Al–Cu eutectic alloy. In this investigation, in addition to GBS and grain rearrangement, extensive interface migration (both grain and phase boundaries) was observed.

Dingley [88] studied the relative motion of grains during superplastic flow and plotted the positions of several individual grain centres relative to an arbitrary origin, as a function of specimen extension. It was shown that grains tend to move along the Affine trajectories* but diverge from them in a random fashion. Further analysis by Hazzledine and Newbury [113] led to the suggestion that during SPD voids will open up at the interface which are filled by grains emerging from

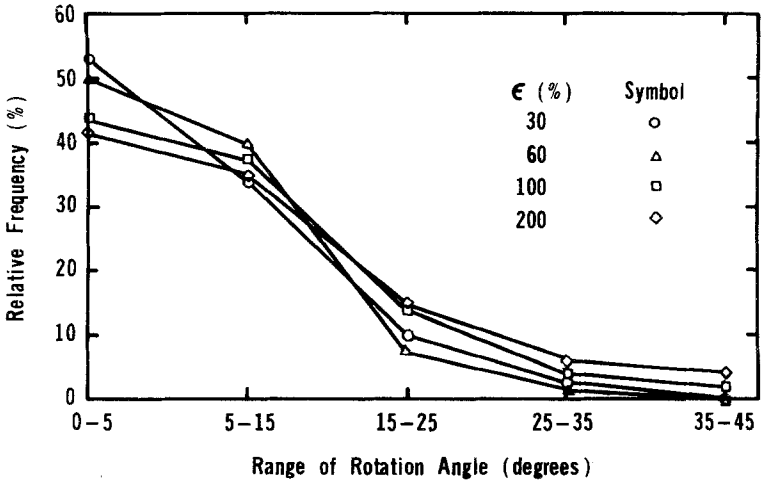

Figure 17 Variation of the extent of grain rotation with strain [63].

*Affine deformation law gives the instantaneous position as a function of the initial position and strains, i.e., for a solid strained in direction $x' = x_0/\epsilon^{1/2}$; $y' = y_0/\epsilon^{1/2}$; and $z' = z_0\epsilon$.

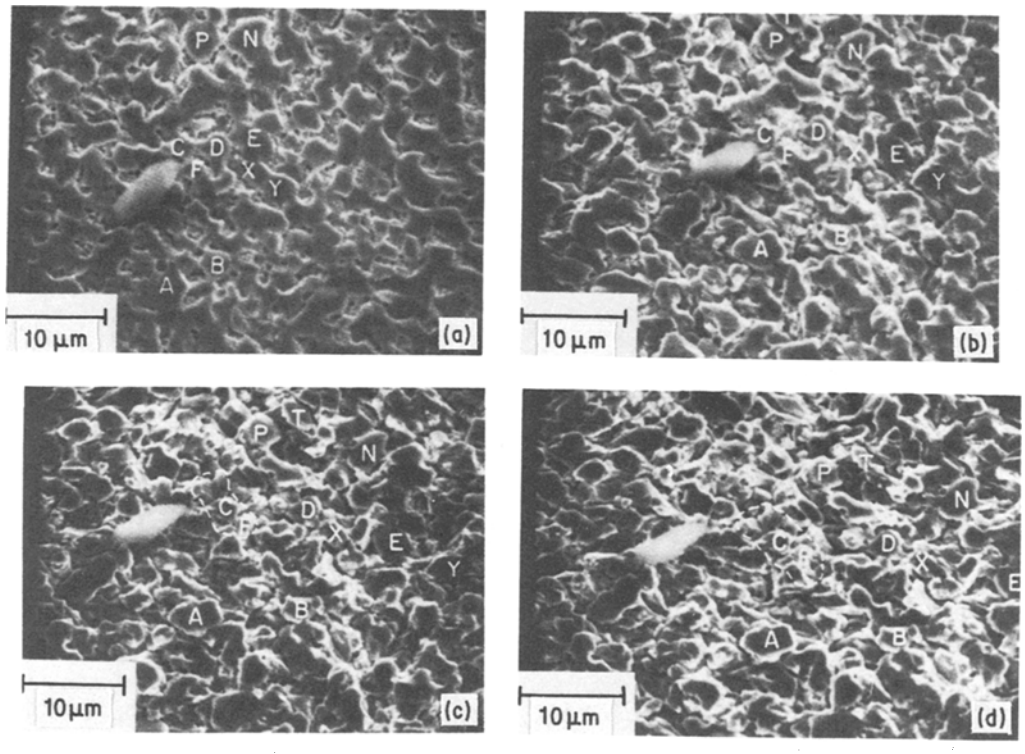

Figure 18 SEM views of grain movements during superplastic deformation of the Pb–Sn eutectic at a strain rate of 10^{-5} sec^{-1} at 25° C: (a) before deformation; (b) after 58% strain; (c) after 98% strain; and (d) after 139% strain. Tension axis is horizontal [109].

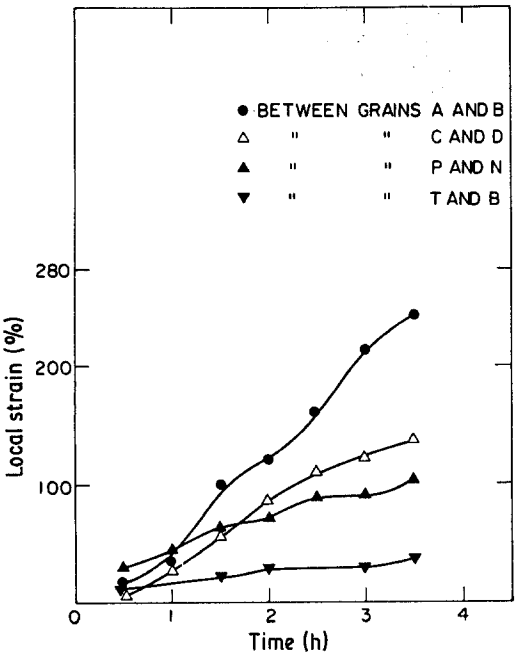

Figure 19 Random component microcreep curves between neighbouring grains of the Pb–Sn eutectic strained to 139% at a strain rate of about 10^{-5} sec^{-1} at 25° C.

the adjacent planes, above and below the plane under consideration. They calculated that at $\epsilon = 0.8$ one third of the grains in the plane section will be new grains emerging from the adjacent planes and at $\epsilon = 1.39$ half of the grains will be new. This sequence is shown in Fig. 21 where the white grains are original grains belonging to a reference plane in the middle of the thickness of specimen and the dark grains are new ones coming from the adjacent planes above or below.

It is worthwhile noting at this point that although this sequence of events in Fig. 21 seems to be supported by experimental results [54, 76, 105], the numerical values quoted above need not always be the same. During SPD the grains do increase their cross-sectional area due to grain growth and GBM, and consequently the number of new grains emerging from adjacent planes will be less than that calculated by Hazzeldine and Newbury. Surface voids which do not extend into the internal layers of the specimen were observed [54, 76, 105] in the early stages of deformation. Fig. 22 shows an emerging grain to fill up the void

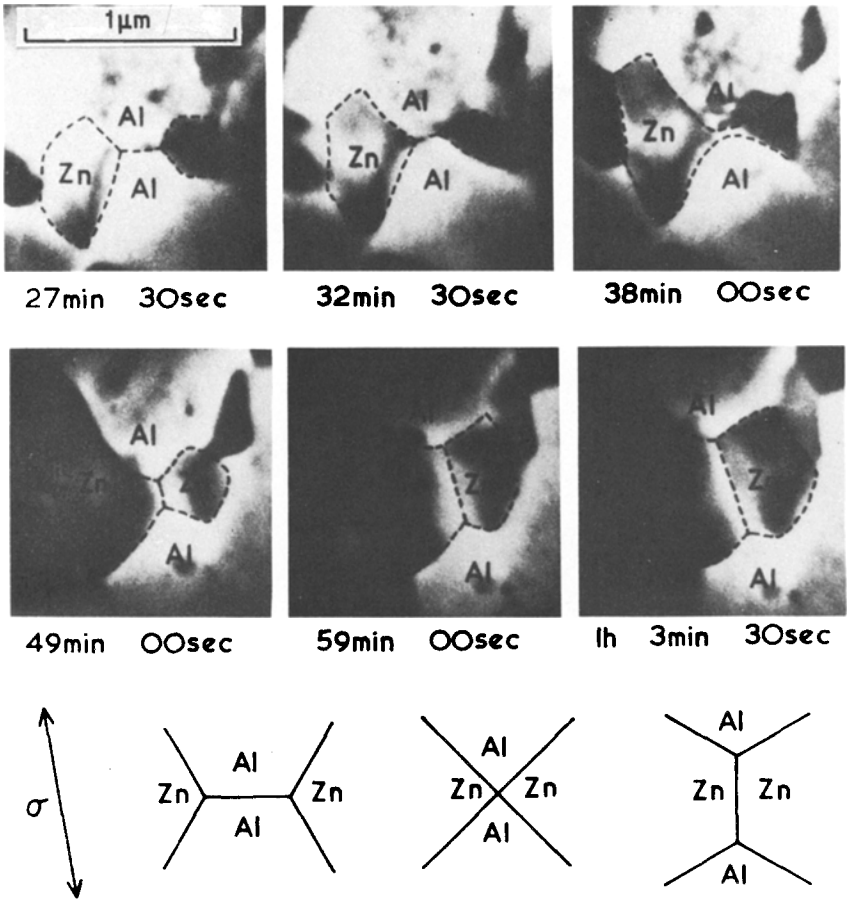

Figure 20 Grain rearrangement during superplastic flow [110].

present on the surface [106]. This new grain also contains distinct slip lines.

4.4. Dislocation activity

It was initially considered that dislocation activity does not occur during SPD. But, in recent years there is mounting evidence of dislocation activity during superplastic flow. These include observations of slip lines on the gage surface [37, 49, 58, 106, 114], stabilization of textures and formation of new textures [29, 32, 61, 63, 65, 66, 115–121] and direct dislocation observation in TEM studies [32, 49, 58, 60, 61, 65, 121, 122]. Still there is debate regarding the existence of dislocation activity. The investigations supporting the dislocation activity are carried out either by using TEM or by following the evolution of textures. The former studies give more insight into the deformation mechanism by relating all active dislocations, including those which accommodate GBS. Texture studies show changes only due to the slip in grain interior under the applied stress. Any investigation that involves both of these techniques will provide a better picture of the total dislocation activity.

4.4.1. TEM studies

The lack of dislocations in TEM examination of thin foils prepared from deformed specimens does not necessarily prove that dislocation mechanisms are not operative during SPD. In fact it emphasizes the problems associated with preservation of the dislocation structure after deformation [60]. Dislocations, if present, might be lost during unloading the specimen at high temperature since the dislocations have only a very short distance to travel before they are annihilated at grain boundaries in fine grain material. Also, some of the dislocations might be lost during preparation of the thin foil. In order to eliminate such problems Nicholson [96] used internal markers to reveal the dislocations which might have been active during

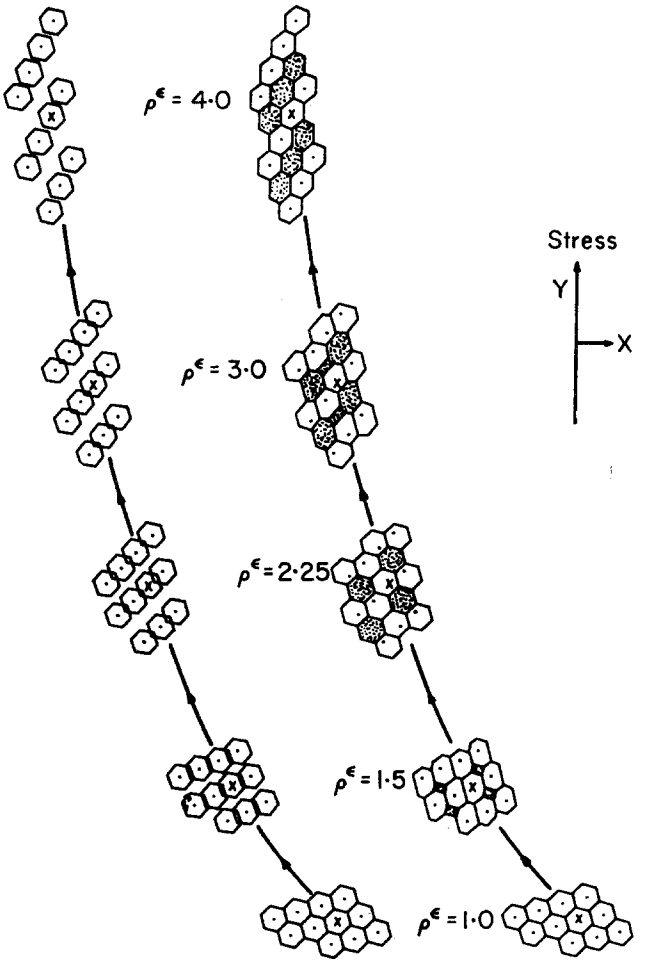

Figure 21 Sequence for three-dimensional grain rearrangement [13].

deformation. He concluded that no dislocation activity accompanied the superplastic flow since the internal markers remained undisturbed. Edington *et al.* [1] showed that the internal markers used by Nicholson had not been effective barriers for dislocations and therefore that experiment did not provide conclusive evidence that dislocations were not active.

In situ tensile straining experiments carried out by Naziri *et al.* [56, 110] also showed either very little or no dislocation activity. However, as demonstrated by Bricknell and Edington [123] under the experimental condition used by Naziri, an extremely high vacancy flux throughout the specimen was created which is not typical for superplastic conditions. This effect which facilitates dislocation climb might have masked or eliminated the evidence of dislocation activity. However, lack of dislocation activity was also reported by Kobayashi *et al.* [112] for an *in situ* experiment on an Al–Cu eutectoid alloy. The conditions selected for this experiment overcame the criticism levelled at Naziri's work. But, it should be noted that their (Kobayashi *et al.*) *in situ* straining was carried out at an initial strain rate of approximately 1.67×10^{-4} sec^{-1} which was shown earlier by Holt and Backofen [124] to be in region I and not in region II. Furthermore, their *in situ* experiment was carried out on thin foils which are not representative of the bulk deformation.

Additional proof about dislocation activity during superplastic flow was found in carefully conducted TEM studies where the tensile specimens were quenched under load [32, 60, 65, 123]. Several investigators [61, 65] reported dislocations being emitted from grain boundaries. Such dislocations can be generated at ledges and protrusions under large stress concentrations due to GBS [125]. Also, in some investigations [65, 122] dislocations were observed to lie in the grain boundaries, but they were shown to be

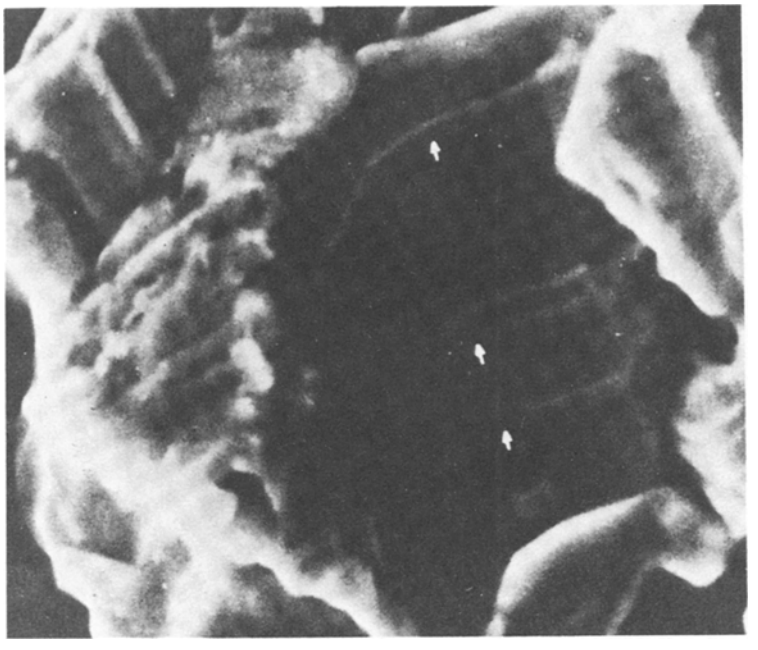

Figure 22 Evidence of dislocation slip in grains emerging to the surface during an *in situ* SEM examination [106].

extrinsic grain boundary dislocations (EGBD) i.e., lattice dislocations lying in the grain boundaries. At the temperatures where the alloy behaved superplastically these dislocations were annihilated at grain boundaries creating non-equilibrium boundaries with higher mobility than the equilibrium boundaries. In a very detailed study of the Al-rich phase of a Zn–40% Al alloy, Samuelsson *et al.* [60] claimed that the dislocations observed after SPD resulted from the deformation. Unfortunately, the comparison of TEM micrographs in Fig. 23 (from the same work) after SPD (Fig. 23a) and after static annealing for the test-period (Fig. 23b) leads to some doubt. In fact, more dislocations are present in the statically annealed specimen than in the superplastically deformed specimen. We believe that the extent of elimination or reduction of the initial high dislocation density may vary depending upon the test conditions and time involved. A more convincing evidence of dislocation activity needs, therefore, to emerge from SPD studies on specimens which contain no (or negligible) dislocations before deformation.

The following TEM studies are being presented in some detail because they cover an extended

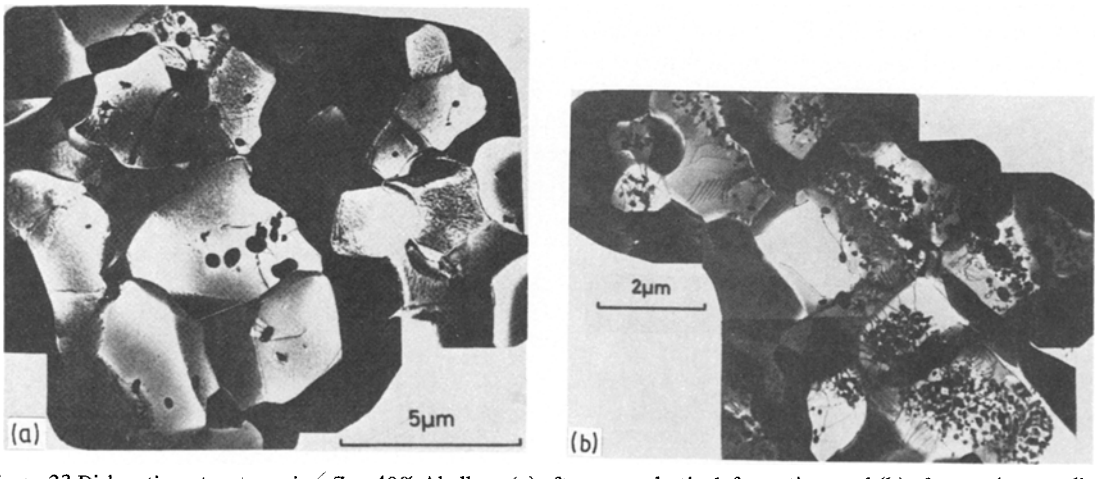

Figure 23 Dislocation structures in a Zn–40% Al alloy: (a) after superplastic deformation; and (b) after static annealing for the time involved in (a) [60].

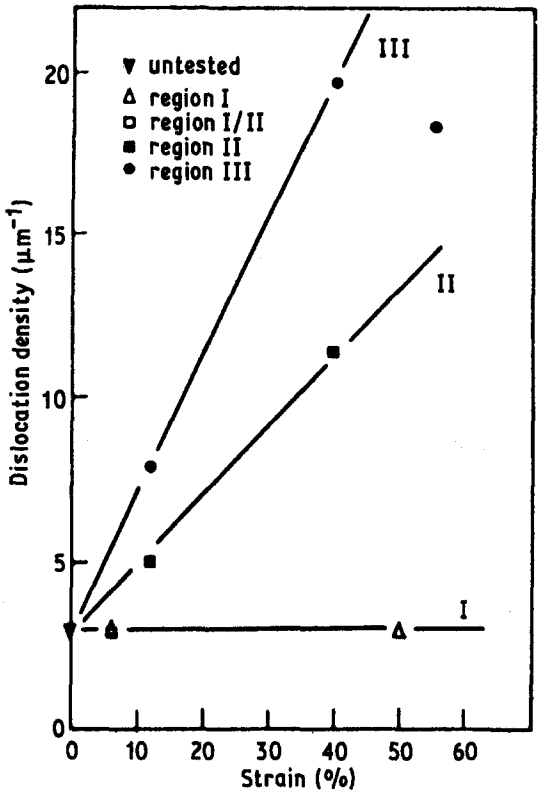

Figure 24 Densities of dislocations in twin boundaries as a function of strain for regions I–III [126].

range of strain rates and also because they provide significant microstructural insight for superplasticity.

The results of measurements of dislocation densities in twin boundaries in the deformed CDA638 alloy (Cu–2.8 Al–1.8 Si–0.4 Co) are shown in Fig. 24 [126]. It was concluded that a large number of matrix dislocations are mobile during deformation in region III. This number diminishes substantially with decreasing stress in region II and is virtually zero in region I. Howell and Dunlop [127] found that overall characteristics of grain boundary dislocations (GBDs) in material deformed in regions I to III were very similar. Fig. 25a shows an array of widely spaced GBDs (12% strain in region II) in the Cu alloy containing a dispersion of precipitates. In the two beam bright field image of Fig. 25a, a number of weakly diffracting dislocations were seen with two intergranular precipitates (arrowed A and B). The interaction between the dislocations and the particles, the former being strongly pinned at both A and B, is shown in Fig. 25b. The dislocations also pile-up at triple junctions and twin boundary intersections. The latter is illustrated in Fig. 25c; the spacing between individual dislocations changes from ~ 10 nm at A to ~ 4 nm at B.

In the Al-rich phase of a Zn–40% Al alloy Samuelsson *et al.* [60] observed that the annealed and undeformed material had a more uniform distribution of the Burger's vectors than the deformed specimens. Most of the dislocations were observed to climb. The dislocation density and proportion of climbing dislocations increased with increasing strain rate, whereas the radius of curvature of the dislocations decreased as the strain rate increased, Fig. 23a. They found that more than one slip system operates within a grain even at the lowest strain rate investigated (lower end of region II). They did not find any sudden change in dislocation structure between region II to region III. Instead, the same type of dislocations seem to operate in both regions. Dislocations were rarely observed lying in or along grain boundaries. However, such dislocations are the ones most likely to be lost during unloading or specimen preparation.

In region III a high dislocation density was produced by deformation. No regular cell structures were formed, only low angle boundaries and dislocation tangles were observed. In the upper end of the region II, dislocations were found in almost every grain containing precipitates, but many grains free of precipitates were also dislocation free. In the specimen deformed at a strain rate corresponding to the middle portion of the region II dislocations were observed almost exclusively in grains containing precipitates. The absence of dislocations in the grains free from precipitates probably points to the difficulty in preserving the dislocation structure for TEM examination. The Burger's vector distribution was similar at all but the lowest strain rate. This might indicate that at this low strain rate the dislocations only accommodate the GBS, whereas at higher strain rates the dislocations contribute also to intragranular slip. In contrast to Fig. 24, the dislocation density and distribution did not change with strain in this investigation. It seems that after some straining at the strain rate under consideration an equilibrium in dislocation density and structure is attained. Kaibyshev and Valiev [128] have noticed the presence of such a transition strain for the equilibrium dislocation density in the SPD of MA8 alloy. The fact that strain-dependent dislocation density is seen in the Cu-alloy (Fig. 24)

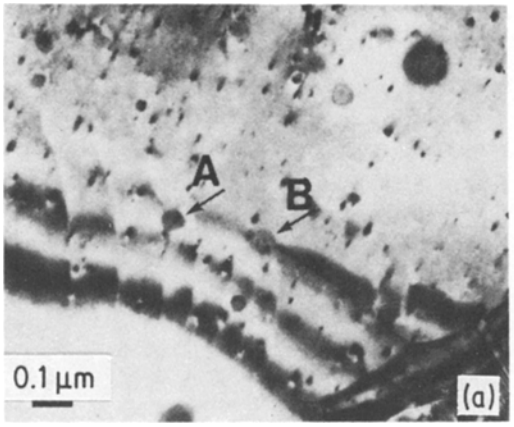

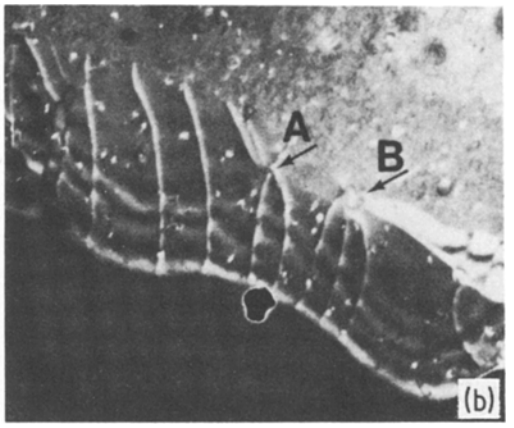

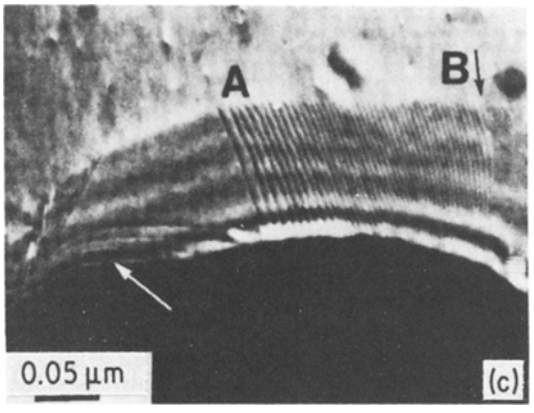

Figure 25 TEM micrographs showing the presence of dislocations during superplastic deformation: (a) interactions between GBDs and precipitates; (b) dark field showing the constriction of GBDs at precipitates: and (c) a pile-up of GBDs against a twin boundary (B). Note also the segments of GBD loops (arrowed in (c)) [127].

whereas a strain-independent dislocation density in Zn–40% Al has been reported by Samuelsson *et al.* [60] may thus be reconciled to such transition strains which depend on the material and the test conditions.

Menzies *et al.* [129] investigated microstructural changes in IN–100 powder-consolidated superalloy over wider range of strain rates (regions I, II and III). The deformed specimens were water quenched in this work. Due to the complex nature of the microstructures it was difficult to differentiate between the defect structures which result from the original extrusion, subsequent annealing or tensile testing. However, the results of interest may be summarized as follows:

1. The microstructure alters markedly during deformation.

2. The dislocation density decreases with decreasing strain rate.

3. The formation or degeneration of low-angle boundaries was noted in regions I and II. The boundaries tended to be fewer and better formed at lower strain rates and frequently occurred near triple points.

4. Extensive dislocation activity was noted in regions I and II but some grains remained dislocation free. The dislocations were often curved and sometimes extended into the matrix.

5. In region III the dislocation density was too high to allow for the resolution of dislocation activity and the time for recovery was too short for well defined low-angle boundaries to be formed.

4.4.2. Texture studies

Texture studies invariably show a reduction in the overall texture due to GBS and grain rotation. In addition to the overall texture reduction, some texture components are stabilized and new ones are created indicating intergranular slip activity [65, 115, 116, 118–120], Fig. 26. The slip behaviour is different not only among different alloys, but also among the different phases present in the same alloy. Cutler *et al.* [119] observed that in an Al–Cu eutectic alloy isolated slip occurs in Al-rich grains deformed in regions I and II mainly in the ⟨100⟩ direction. As the strain rate is increased, i.e., region III, there is a change from a skeleton tube component to a ⟨111⟩ fibre texture indicative of multiple slip. The slip is easier in the Al-rich phase in the ⟨100⟩ direction (Schmidt factor = 0.408) than in the ⟨111⟩ direction (Schmidt factor = 0.272). Hence, the ⟨111⟩ fibre texture will be more stable than the ⟨111⟩ texture component. In the Al_2Cu phase there is

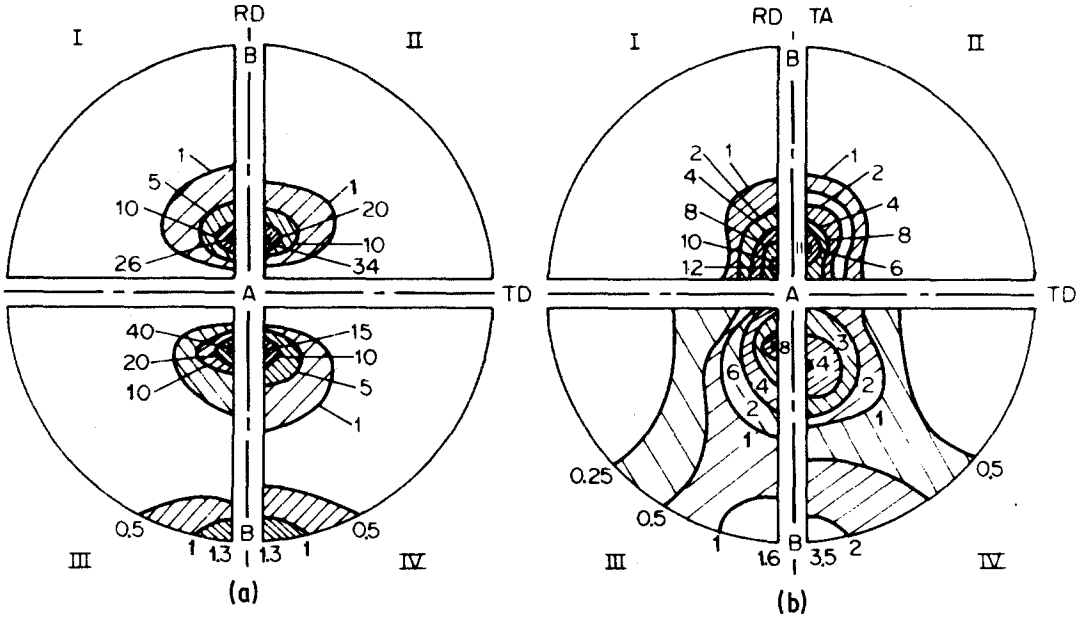

Figure 26 (0001) pole figures for the Zn-phase of Zn–Al alloys (I) Zn–2% Al; (II) Zn–10% Al; (III) Zn–22% Al; (IV) Zn–50% Al. (a) Undeformed; (b) strained 30% at 523 K and $\dot{\epsilon} = 2 \times 10^{-2}$ sec^{-1} [65].

an initial decrease in texture up to 50% strain and subsequently an increase in texture, predominantly the {100} ⟨*uvo*⟩ component, at larger strains.

For the Zn–Al alloys the texture developed during SPD depends on the alloy composition [65]. For the alloys containing up to 22% Al [61, 65, 117, 120] there are indications of single {0001} ⟨11$\bar{2}$0⟩ basal slip at low strain rates (region I and the lower part of region II) with gradual transition to multiple slip, i.e., prismatic {01$\bar{1}$0} plane slip or pyramidal ⟨1123⟩ slip in addition to the basal slip, at higher strain rates (the upper part of region II and region III). The transition from single to multiple slip in the Zn–22Al eutectoid was found to be a function of grain size, i.e., the larger the grain size, the lower the transition strain rate. For higher aluminum contents ($\geqslant$ 40% Al), at low strain rates (region I and lower part of region II) there is a prismatic {0 1 $\bar{1}$ 0} plane slip in the Zn-rich phase with gradual transition to multiple slip (prismatic and basal) at high strain rates [65]. In the Al-rich phase the {1 1 0} ⟨001⟩ texture component was retained in both regions II and III indicating that some slip occurred at all strain rates [118]. Retention of the skeleton tube of the texture in region III shows that multiple slip occurred in this region, whereas only single slip occurred in region II. Similar results were obtained for an Al–9Zn–1Mg alloy [63], Sn–Pb [7] and a Mg–1.5Mo–0.3Ce alloy [32].

4.5. Diffusional process and unique topological features

Although GBS is the predominant mechanism of SPD, the diffusional process appears to be equally important as seen in Fig. 9. The contribution of the diffusional process to SPD decreases with increasing strain rates. Microstructural study of superplastically deformed specimens exhibit some unique features due to the diffusional process alone or due to its combination with other operating mechanisms. Some of the more interesting observations on this aspect are described below while the formation of precipitate free zones has been discussed under Section 4.2.

4.5.1. Grain boundary features and grain shape

The interfaces (both grain and phase boundaries) appear, before deformation, as straight lines. After deformation, the interfaces have a curved aspect [6, 9, 19–21, 35–37]. In an *in situ* TEM study, Naziri *et al.* [56] observed that the initially straight boundaries remain straight in the undeformed grip region of the specimen but become curved in the deformed region of the specimen, as shown in Figs. 14a and 14b respectively. Other observations

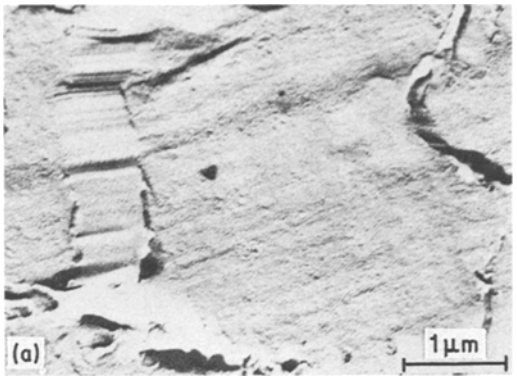

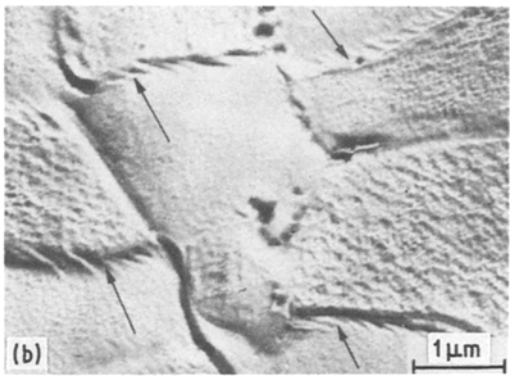

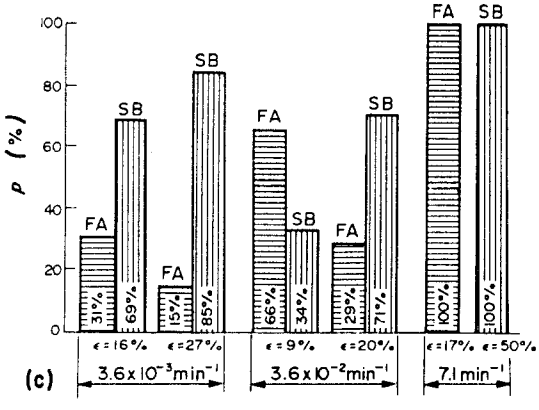

Figure 27 Topographical features of Zn–22% Al eutectoid due to superplastic deformation [91]; (a) The striated band on the grain boundary (unetched) at 250° C, $\epsilon = 30\%$, $\dot{\epsilon} = 6 \times 10^{-4}$ sec^{-1}. (b) Narrow folded areas along grain boundaries at 250° C, $\epsilon = 9\%$, $\dot{\epsilon} = 1.67 \times 10^{-4}$ sec^{-1}. (c) The relative frequency formation of "classical" striated bands (SB) and narrow folded areas (FA) on grain boundaries at different strains and strain rates at 250° C.

[99] show that not only the overall shape of the interphase boundaries becomes curved, but many local deviations from the straightness can be seen in the interphase boundaries giving rise to a "bulbous" aspect, Fig. 14c. The curvatures in the boundaries of the superplastically deformed specimen disappear by subsequent static annealing [20]. The formation of curved boundaries has been associated with localized grain boundary migration [99].

There is evidence of transient grain shape change during deformation which occurs in a narrow region near the grain boundaries [32, 34, 39, 46, 49, 56, 63, 105]. The deformed regions near the interfaces appear under a microscope (probably, due to the lower magnification often used) as thickened boundaries or as heavily grooved regions with deep gouged markings. A microstructural feature related to such markings will be described later in detail as a "striated" band. The width of the deformed regions near the boundaries increases as the strain rate decreases [32, 34]. Also, after reannealing at the test temperature, the deformed regions disappear [34] in a manner similar to the boundary curvature.

Post-deformation metallographic examination also reveals a tendency for the grains of the same phase to cluster [7, 23, 29, 30, 38, 49], especially at low strain rates, i.e., region I [30, 49], and high strain rates, i.e., region III [106].

4.5.2. Striated bands

In several works [24, 46, 49, 50, 56, 91, 98, 114, 130] regions with characteristic strips at grain boundaries called striated bands (SB) of deformation zones were discovered while investigating the surfaces of deformed specimens of different alloys using a replica method. A detailed quantitative work was undertaken to investigate SB in a Zn–22% Al alloy by Novikov *et al.* [91]. The observations from this investigation are presented below.

1. Striated bands appear on the flat polished surface only after deformation. As shown in Fig. 27a, SB is a corrugated grooved surface of the areas that stand out in relief. They are separated from grains by clear-cut boundaries which are geometrically somewhat similar to each other. Inside the banded strips, the grooves and crests of the relief are oriented at small angles to their boundaries.

2. The total length of grain boundaries with SB increases with increasing strain and increasing strain rate. There appears also some narrow folded areas (FA), Fig. 27b, along the grain boundaries. The FA are suggested to be the initial stage of SB

TABLE VII The relative part (%) of different types of grain boundaries with SB after specimen tension with different strains and strain rates [91]

$\dot{\epsilon}$ (sec^{-1})	ϵ (%)	Boundary type		
		α/β	β/β	α/α
6.0×10^{-6}	20	51	26	23
6.0×10^{-5}	7	71	24	5
	21	63	36	1
	29	68	27	5
6.0×10^{-4}	9	71	29	–
	20	57	38	5
1.7×10^{-2}	17	85	15	–
1.2×10^{-1}	50	62	30	8
	35	67	20	13

formation since the latter increases at the expense of the former with increasing strain as shown in Fig. 27c.

3. The striated bands are formed preferentially on the interphase boundaries α/β and grain boundaries β/β in this alloy. The proportions of the SB at different types of boundaries at different strain rates and strains are listed in Table VII. The width of the SB increases at the same rate as the rate of phase growth.

4. It has been suggested that these striated bands are formed as a result of diffusion (oriented mass transfer consisting of a solution–precipitation process) creep and GBS.

4.5.3. Formation of new grains during SPD

Generally, SPD causes grain growth in equiaxed microstructures. However, at higher strain rates corresponding to region III recrystallization is also seen in some materials.

If the SB are growths on or extensions of the original grains then considerable grain elongation in the direction of tensile axis may be anticipated after SPD. But the grains in various alloys do not show an extension more than 1.2 to 1.5 times the initial size even after several hundred % elongation of the specimen. The retention of equiaxed grain shape is then possible only by elimination of the SB or by formation of new grains. Portnoy *et al.* [131] have recently reported formation of new grains at deformation zone during SPD of the Zn–22% Al alloy. Fig. 28 illustrates the appearance of a new grain 3 between grains 1 and 2 after SPD through the formation of SB. The formation of the SB seems to be an opposite phenomena of cavity formation in an intermediate stage during grain rearrangement in SPD. The SB are predominantly formed at boundaries which are approximately at right angles to the tensile axis.

The photomicrographs taken sequentially in the same place before SPD, after SPD and after lightly etching the superplastically deformed specimen revealed the formation of new grains on transverse grain boundaries, increasing in number with the degree of deformation. Table VIII shows the increase in the number of grains and the deformation zone with increasing strain.

This type of formation of new grains during SPD has been attributed [131] to a special kind of diffusion creep involving dissolution–

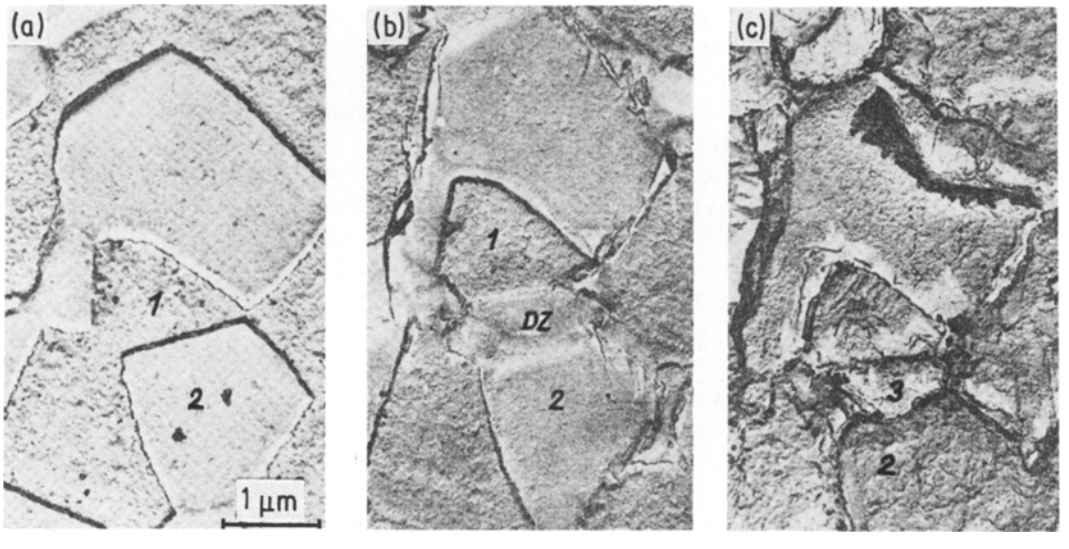

Figure 28 Appearance of a new grain (3) on a α/β boundary of Zn–22% Al eutectoid [131]: (a) before SPD; (b) after SPD; and (c) after further etching.

TABLE VIII Appearance of new grains and deformation zones at different strain levels after SPD at 250° C and initial $\dot{\epsilon} = 1.7 \times 10^{-3}$ sec^{-1}

ϵ (%)	Increase in the number of grains (%)	Number of deformation zones	Ratio $\frac{\text{increase in number of grains}}{\text{number of deformation zones}}$ (%)
25	17	20	35
35	28	24	46
47	34	25	56

precipitation processes. Fig. 29 schematically shows the formation of new grains (β phase) by a flux of atoms from the decomposing third grain (β phase) on to the transverse boundary between two α grains.

The microstructural observations presented here reveal several unique features developed during SPD and the microstructural changes are very heterogeneous. The structure–property correlations treated in the literature, on the other hand, are concerned mainly with the grain size and only occasionally with the grain shape. This points to the inadequacy of the usual practice of using the grain (or phase) size as the only significant microstructural parameter in the constitutive equation for superplastic flow.

5. Summary and conclusions

From the foregoing presentation it is evident that a somewhat common microstructural pattern emerges for all the materials and testing conditions investigated in conjunction with superplastic deformation phenomenon. The major microstructural characteristics of superplasticity are:

1. The microstructure, if not equiaxed and homogeneous from the onset of the deformation, becomes nearly equiaxed and uniform during the first few tens % of strain. However, no recrystallization in the usual sense occurs.
2. Even after hundreds and thousands % strain, grains remain essentially equiaxed.
3. Previously straight interfaces (both grain and phase boundaries) become curved, and sometimes the phase boundaries have a bulbous aspect.
4. There is strain-enhanced grain growth with maximum sensitivity at intermediate strain rates.
5. Deformation zones are formed on boundaries approximately perpendicular to the axis of tension.
6. Extensive grain boundary migration and grain boundary sliding occur.
7. There are large relative rotations of individual grains and groups of grains.
8. Three-dimensional grain rearrangements take place during superplastic flow.
9. Considerable dislocation activity occurs during superplastic flow. Dislocations are generated at or near boundaries and are annihilated in the boundaries.

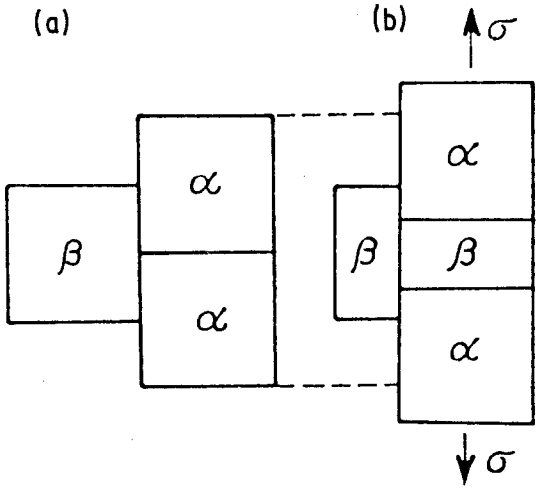

Figure 29 Schematic diagram showing the formation of a new grain during diffusion creep involving dissolution–precipitation processes: (a) before; and (b) after SPD [131].

Acknowledgement

This work was partly supported by grants from the US National Science Foundation and from the US Department of Energy.

References

1. J. W. EDINGTON, K. N. MELTON and C. P. CUTLER, *Prog. Mater. Sci.* **21** (1976) 61.
2. A. K. MUKHERJEE, *Ann. Rev. Mater. Sci.* 9 (1979) 191.
3. D. M. R. TAPLIN, G. L. DUNLOP and T. G. LANGDON, *ibid* 9 (1979) 151.
4. K. A. PADMANABHAN and G. J. DAVIES, in "Superplasticity" (Springer-Verlag, New York, 1980).
5. S. SAGAT and D. M. R. TAPLIN, *Met. Sci.* 5 (1976) 94.
6. M. J. STOWELL, J. L. ROBERTSON and B. M. WATTS, *Met. Sci. J.* 3 (1969) 41.

7. C. P. CUTLER and J. W. EDINGTON, *Scripta Metall.* **5** (1971) 201.
8. M. SUERY and B. BAUDELET, *J. Mater. Sci.* **10** (1975) 22.
9. B. M. WATTS and M. J. STOWELL, *ibid.* 6 (1971) 228.
10. A. ARIELI and A. ROSEN, *Met. Trans.* **8A** (1977) 1591.
11. G. HERRIOT, B. BAUDELET and J. J. JONAS, *Acta Metall.* **24** (1976) 687.
12. C. I. SMITH, B. NORGATE and N. RIDLEY, *Met. Sci.* **5** (1976) 182.
13. G. HERRIOT, M. SUERY and B. BAUDELET, *Scripta Metall.* **6** (1972) 657.
14. S. SAGAT and D. M. R. TAPLIN, *Acta Metall.* **24** (1976) 307.
15. H. W. HAYDEN, S. FLOREEN and P. D. GODDELL, *Met. Trans.* **3** (1972) 833.
16. C. HOMER, J. P. LECHTEN and B. BAUDELET, *Met. Trans.* **8A** (1977) 1191.
17. B. P. KASHYAP, PhD thesis, Indian Institute of Technology, Kanpur, 1980.
18. E. E. UNDERWOOD, in "Quantitative Microscopy" edited by R. T. DeHoff and F. N. Rhines (McGraw-Hill Book Co, New York, 1968) p. 77.
19. M. SUERY and B. BAUDELET, *Rev. Phys. Appl.* **19** (1978) 53.
20. B. M. WATTS, M. J. STOWELL, B. L. BAIKIE and D. G. E. OWEN, *Met. Sci.* **5** (1976) 198.
21. G. RAI and N. J. GRANT, *Met. Trans.* **6A** (1975) 385.
22. S. T. LAM, A. ARIELI and A. K. MUKHERJEE, *Mater. Sci. Eng.* **40** (1979) 73.
23. T. H. ALDEN and H. W. SCHADLER, *TMS-AIME* **242** (1968) 825.
24. D. LEE, *Met. Trans.* **1** (1970) 309.
25. R. C. GIFKINS, *ibid.* **8A** (1977) 1507.
26. W. B. MORRISON, *Trans. ASM* **61** (1968) 423.
27. H. W. HAYDEN, R. C. GIBSON and J. H. BROPHY, *ibid.* **60** (1967) 3.
28. K. NUTTAL, *Scripta Metall.* **10** (1976) 835.
29. O. A. KAIBYSHEV, I. V. KAZACHKOV and V. M. ROZENBERG, *Fiz. Metal. Metalloved.* **36** (1973) 1235.
30. A. ARIELI, A. YU and A. K. MUKHERJEE, *Met. Trans.* **11A** (1980) 181.
31. R. Z. VALIEV and O. Z. KAIBYSHEV, *Fiz. Metal. Metalloved.* **41** (1976) 382.
32. *Idem, Phys. Status. Solidi* **44(a)** (1977) 65.
33. P. GRIFFITH and C. HAMMOND, *Acta Metall.* **20** (1972) 935.
34. J. D. LEE and P. NIESSEN, *J. Mater. Sci.* **9** (1974) 1467.
35. A. K. GHOSH and C. H. HAMILTON, *Met. Trans.* **10A** (1979) 699.
36. A. M. GARDE, H. M. CHUNG and T. F. KASSNER, *Acta Metall.* **26** (1978) 151.
37. D. L. HOLT, *TMS-AIME* **242** (1968) 25.
38. C. M. PACKER and O. D. SHERBY, *Trans. ASM* **60** (1967) 21.
39. T. H. ALDEN, *Acta Metall.* **15** (1967) 469.
40. D. LEE and W. A. BACKOFEN, *TMS-AIME* **239** (1967) 1034.
41. P. CHAUDHARI, *Acta Metall.* **15** (1967) 1777.
42. H. W. HAYDEN and J. H. BROPHY, *Trans. ASM* **61** (1968) 542.
43. K. NUTTAL and R. B. NICHOLSON, *Phil. Mag.* **17** (1968) 1087.
44. W. B. MORRISON, *Trans. ASM* **61** (1968) 423.
45. *Idem, TMS-AIME* **242** (1968) 2221.
46. D. LEE, *Acta Metall.* **17** (1969) 1057.
47. H. NAZIRI and R. PEARCE, *Scripta Metall.* **3** (1969) 811.
48. R. J. LINDINGER, R. C. GIBSON and J. H. BROPHY, *Trans. ASM* **62** (1969) 230.
49. G. L. DUNLOP and D. M. R. TAPLIN, *J. Mater. Sci.* 7 (1972) 316.
50. A. KARIM and W. A. BACKOFEN, *Met. Trans.* **3** (1972) 709.
51. S. SAGAT, P. BLENKINSOP and D. M. R. TAPLIN, *J. Inst. Metals* **100** (1972) 268.
52. M. A. CLARK and T. H. ALDEN, *Acta Metall.* **21** (1973) 1195.
53. M. L. VAIDYA, K. L. MURTY and J. E. DORN, *ibid.* **21** (1973) 1615.
54. H. NAZIRI and R. PEARCE, *ibid.* **22** (1974) 1321.
55. M. OTSUKA, Y. MIURA and R. HORIUCHI, *Scripta Metall.* 8 (1974) 1405.
56. H. NAZIRI, R. PEARCE, M. HENDERSON-BROWN and K. F. HALE, *Acta Metall.* **23** (1975) 489.
57. K. N. MELTON, C. P. CUTLER and J. W. EDINGTON, *Scripta Metall.* **9** (1975) 515.
58. S. C. MISRO and A. K. MUKHERJEE, in International Symposium on Rate Processes in Plastic Deformation, Cleveland, 1972, edited by J. C. M. Li and A. K. Mukherjee (ASM, Metals Park, Ohio, 1975) p. 434.
59. M. D. C. MOLES and G. J. DAVIES, *Scripta Metall.* **10** (1976) 455.
60. L. C. A. SAMUELSSON, K. N. MELTON and J. W. EDINGTON, *Acta Metall.* **24** (1976) 1017.
61. O. A. KAIBYSHEV, R. Z. VALIEV and V. V. ASTANIN, *Phys. Status. Solidi* **35 (a)** (1976) 403.
62. D. G. ATTWOOD and P. M. HAZZELDINE, in Proceedings of the 4th International Conference on Strength of Metals and Alloys, Vol. 1, Nancy, France, (1976) p. 413.
63. K. MATSUKI, H. MONITA, M. YAMADA and Y. MURAKAMI, *Met. Sci.* **6** (1977) 156.
64. D. W. LIVESEY and N. RIDLEY, *Met. Trans.* **9A** (1978) 519.
65. O. A. KAIBYSHEV, I. V. KAZACHOV and S. YA. SALIKHOV, *Acta Metall.* **26** (1978) 1887.
66. A. ARIELI and A. K. MUKHERJEE, *Mater. Sci. Eng.* **43** (1980) 47.
67. R. K. AUBAKIROVA, V. A. LIKHACHEV, M. M. MYSHLYAYEV, A. A. PRESN'YAKOV and D. R. CHALAYEV, *Phys. Met. Metall.* **51** (1981) 172.
68. D. W. LIVESTY and N. RIDLEY, *J. Mater. Sci.* **17** (1982) 2257.
69. B. P. KASHYAP and G. S. MURTY, *ibid.* **18** (1983) 2063.
70. B. P. KASHYAP and A. K. MUKHERJEE, *ibid.* **18** (1983) 3299.
71. C. H. CACERES and D. S. WILKINSON, *Acta Metall.* **32** (1984) 415.

72. G. GUREWITZ, PhD thesis, University of California, Davis, 1984.
73. A. ARIELI and A. K. MUKHERJEE, *Scripta Metall.* **13** (1979) 331.
74. D. S. WILKINSON and C. H. CACERES, *J. Mater. Sci. Lett.* **3** (1984) 395.
75. O. A. KAIBYSHEV, I. V. KAZACHKOV, V. V. ASTANIN and B. V. RODIONOV, *Izv. vuzov. Tsvetnaya Metallurgia* **3** (1974) 127.
76. P. M. HAZZELDINE and D. E. NEWBURY, in "Grain Boundary Structure and Properties" edited by G. A. Chadwick and D. A. Smith (Academic Press, London, 1975) p. 235.
77. S. L. SEMIATIN, J. F. THOMAS Jr and P. DADRAS, *Met. Trans.* **14A** (1983) 2363.
78. A. DUTTA, N. C. BIRLA and A. K. GUPTA, *Trans. Indian Inst. Met.* **36** (1983) 169.
79. P. DADRAS and J. F. THOMAS Jr, *Met. Trans.* **12A** (1981) 1867.
80. O. A. KAIBYSHEV, *Czech. J. Phys.* **31** (1981) 223.
81. K. MATSUKI, N. HARIYAMA, M. TOKIZAWA and Y. MURAKAMI, *Met. Sci.* **17** (1983) 503.
82. I. M. LIFSHITZ, *Soviet Phys.* **17** (1963) 989.
83. G. B. GIBBS, *Mem. Sci. Rev. Met.* **62** (1965) 781.
84. R. C. GIFKINS and T. G. LANGDON, *Scripta Metall.* **4** (1970) 563.
85. R. RAJ and M. F. ASHBY, *Met. Trans.* **2** (1971) 1113.
86. S. HORI, N. FURUSHIRO and S. KAWAGUCHI, in Proceedings of the 19th Japan Congress on Material Research, Kyoto, Japan, 1976 (The Society of Materials Science, Kyoto, 1976) p. 1.
87. K. MATSUKI, Y. UENO and M. YAMADA, *J. Jpn. Inst. Metals* **38** (1974) 219.
88. D. J. DINGLEY, in 4th Annual Scanning Electron Microscopy Conference (Illinois Institute of Technology, Research Institute, Chicago, 1970) p. 329.
89. R. B. VASTAVA and T. G. LANGDON, *Acta Metall.* **27** (1979) 251.
90. N. FURUSHIRO and S. HORI, *Scripta Metall.* **13** (1979) 653.
91. I. I. NOVIKOV, V. K. PORTNOY and T. E. TERENTIEVA, *Acta Metall.* **25** (1977) 1139.
92. P. SHARIAT, R. B. VASTAVA and T. G. LANGDON, *ibid.* **30** (1982) 285.
93. H. GLEITER and B. CHALMERS, *Prog. Mater. Sci.* **16** (1972) 179.
94. T. CHANDRA, J. J. JONAS and D. M. R. TAPLIN, *J. Mater. Sci.* **13** (1978) 2380.
95. M. F. ASHBY, *Surf. Sci.* **31** (1972) 498.
96. R. B. NICHOLSON, in "Electron Microscopy and Structure of Materials" edited by G. Thomas (University of California Press, Berkeley, 1972) p. 689.
97. H. E. CLINE and T. H. ALDEN, *TMS-AIME* **239** (1967) 710.
98. A. KARIM, D. L. HOLT and W. A. BACKOFEN, *ibid.* **245** (1969) 1131.
99. R. H. JOHNSON, C. M. PACKER, L. ANDERSON and O. D. SHERBY, *Phil. Mag.* **18** (1968) 1309.
100. R. E. REED-HILL, in "Physical Metallurgy Principles" (D. Van Nostrand Co, Inc, Princeton, New Jersey, 1966) p. 216.
101. A. M. KING and D. A. SMITH, *Met. Sci.* **8** (1979) 113.
102. C. J. SIMPSON, W. C. WINEGARD and K. T. AUST, in "Grain Boundary Structure and Properties" edited by G. A. Chadwick and D. A. Smith (Academic Press, London, 1975) p. 201.
103. K. SMIDODA, C. GOTTSCHALK and M. GLEITER, *Acta Metall.* **26** (1978) 1833.
104. *Idem, Met. Sci.* **8** (1979) 146.
105. A. E. GECKINLI and C. R. BARRET, *J. Mater. Sci.* **11** (1976) 510.
106. W. HATZ, E. RUEDL and P. SHILLER, *ibid.* **10** (1975) 2003.
107. C. R. BARRETT, in "Third Nordic High Temperature Symposium" edited by J. G. Rasmunsen (Polyteknisk Forlag, Copenhagen, 1972) p. 79.
108. W. BEERE, *J. Mater. Sci.* **12** (1977) 2093.
109. G. RAI and N. J. GRANT, *Met. Trans.* **14A** (1983) 1451.
110. H. NAZIRI, R. PEARCE, M. HENDERSON BROWN and K. F. HAKE, *J. Microsc.* **97** (1973) 229.
111. M. F. ASHBY and R. A. VERRALL, *Acta Metall.* **21** (1973) 149.
112. Y. KOBAYASHI, Y. ISHIDA and M. KATO, *Scripta Metall.* **11** (1977) 51.
113. P. M. HAZZELDINE and D. E. NEWBURY, in Proceedings of the 3rd International Conference on Strength of Metals and Alloys, Cambridge, 1973, Vol. I (Institute of Metals, London, 1973) p. 202.
114. A. BALL and M. M. HUTCHINSON, *Met. Sci. J.* **3** (1969) 1.
115. C. M. PARKER, R. H. JOHNSON and O. D. SHERBY, *TMS-AIME* **242** (1968) 2485.
116. H. NAZIRI and R. PEARCE, *J. Inst. Metals* **98** (1970) 71.
117. O. A. KAYBYSHEV and I. V. KAZACHOV, *Fiz. Metal. Metalloved.* **34** (1972) 396.
118. K. N. MELTON, C. P. CUTLER, J. S. KALLEND and J. W. EDINGTON, *Acta Metall.* **22** (1974) 165.
119. C. P. CUTLER, J. W. EDINGTON, J. S. KALLEND and K. N. MELTON, *ibid.* **22** (1974) 655.
120. K. N. MELTON and J. W. EDINGTON, *Scripta Metall.* **8** (1974) 1141.
121. K. MATSUKI, Y. UETANI, M. YAMADA and Y. MURAKAMI, *Met. Sci.* **5** (1976) 235.
122. R. Z. VALIEV and O. A. KAYBYSHEV, *Phys. Status Solidi* **44 (a)** (1977) 477.
123. R. M. BRICKNELL and J. W. EDINGTON, *Acta Metall.* **25** (1977) 447.
124. D. L. HOLT and W. A. BACKOFEN, *Trans. ASM* **59** (1966) 755.
125. L. E. MURR, in "Interfacial Phenomena in Metals and Alloys" (Addison-Wesley Publishing Co, Massachusetts, 1975) p. 338.
126. L. FALK, G. L. DUNLOP and T. G. LANGDON, in Proceedings of the 7th European Congress on Electron Microscopy, (The Hague, Electron Microscopy, 1980) p. 154.
127. P. R. HOWELL and G. L. DUNLOP, in Creep and Fracture of Engineering Materials and Structures, International Conference University College Swansea, edited by B. Wilshire and D. R. J. Owen (Pineridge Press, Swansea, 1981) p. 127.

128. O. A. KAIBYSHEV and R. Z. VALIEV, *Res. Mechanica* **3** (1981) 23.
129. R. G. MENZIES, G. J. DAVIES and J. W. EDINGTON, *Met. Sci.* **16** (1982) 483.
130. S. W. ZEHR and W. A. BACKOFEN, *Trans. ASM* **61** (1968) 300.
131. V. K. PORTNOY, I. I. NOVIKOV and V. S. LEVCHENKO, *Phys. Met. Metall.* **51** (1981) 164.

Received 3 October
and accepted 2 November 1984